Unland, Ellen ; Miramontes, Elda ; Spieß, Volkhard ; Bozzano, Graziella ; Kasten, Sabine ; Schwenk, Tilmann

Evolution of a buried moat-drift system in the Ewing Terrace uncovering highly dynamic bottom currents at the Argentine margin from the early Oligocene to middle Miocene

Journal Article as: peer-reviewed accepted version (Postprint)

DOI of this document*(secondary publication): https://doi.org/10.26092/elib/3510

Publication date of this document: 04/12/2024

* for better findability or for reliable citation

Evolution of a buried moat-drift system within the Ewing Terrace uncovering highly dynamic bottom-currents at the Argentine Margin during Early Oligocene to Middle Miocene.

Ellen Unland[1,6*], Elda Miramontes[1,2], Volkhard Spiess[1,2], Graziella Bozzano[3,4], Sabine Kasten[1,2,5], Tilmann Schwenk[1,2]

[1] Faculty of Geosciences, University of Bremen, Bremen, Germany

[2] MARUM – Center for Marine Environmental Sciences, University of Bremen, Germany

[3] Department of Oceanography, Argentine Hydrographic Service (SHN), Buenos Aires, Argentina

[4] CONICET, Buenos Aires, Argentina

[5] Alfred Wegener Institute Helmholtz Centre for Polar and Marine Research, Bremerhaven, Germany

[*] Corresponding author: Ellen Unland (eunland@uni-bremen.de)

[6]now at Department of Geology, University of Otago, Dunedin, Aotearoa New Zealand

ABSTRACT

The Ewing Terrace is a relatively flat surface formed by the action of bottom-currents and part of a Contourite Depositional System (CDS) at the Argentine continental slope. It is situated in a highly complex oceanographic setting at the Brazil-Malvinas Confluence Zone. Located in water depths of ~1000–1200 m and incised by the Mar del Plata Canyon, the Ewing Terrace is separated into the Northern Ewing Terrace (NET) and the Southern Ewing Terrace (SET). The long-term variations in ocean circulation led to a complex internal architecture of the terrace. As a result, this region represents a unique archive for studying sedimentary features that were eroded, transported, and deposited by along- and down-slope processes.

An in-depth data analysis of high-resolution multichannel seismic profiles exhibits a complex sequence of erosional and depositional contouritic features, namely buried moat-drift systems identified in depths of ~ 370-750 m below the seafloor. They are arranged in migrating sequences and clustered in the Early Oligocene to Middle Miocene. This pattern is probably attributable to the vertical shift of water masses and to a highly dynamic oceanographic setting with spatial changes influenced by the Brazil-Malvinas Confluence Zone over this particular geological time.

The moat-drift systems reveal significant lateral changes from north to south. In the southern area of the SET, the moats are constructional, and the associated separated mounded drifts are well developed. In contrast, the northern area exhibits two types of moats, reminiscent of cut-and-fill structures that mirror the significant and rapid changes in bottom current dynamics.

With these new insights, this study contributes to a better understanding of moat-drift systems and improves the knowledge about past oceanographic dynamics and sediment deposition at the northern Argentine margin.

INTRODUCTION

Contourites are defined as sediments that are "deposited or substantially reworked by the persistent action of bottom-currents" (Stow et al., 2002; Rebesco et al., 2008, 2014; Smillie et al., 2018). The geometry of contourites depends on several factors, such as bottom current strength and distribution, topography and sediment availability (Miramontes et al., 2021; Wilckens et al., 2023a,b). Particularly strong bottom-currents are able of reworking, winnowing, and eroding the seafloor and subsequently preventing deposition, while low flow velocities favor accumulation, resulting in the formation of different types of contourites (Miramontes et al., 2021). According to the bottom current speed, slope angle of the margin, and sediment availability, deposits are differentiated between erosional, depositional or mixed erosional-depositional features and can be found along continental margins and abyssal plains all over the world (Thiéblemont et al., 2019; Stow and Smillie, 2020; Kirby et al., 2021; Rodrigues et al., 2022). Hence, systems that comprise the aforementioned features are so-called Contourite Depositional Systems (CDS; Hernández-Molina et al., 2009).

Erosional features associated with a CDS develop incisions that are often strongly related to high-energy bottom-currents and are usually under a bottom current core (Hernandéz-Molina et al., 2008; García et al., 2009; Smillie et al., 2018; Miramontes et al., 2021). Moats and contourite channels are both incisions parallel to the bathymetric contourites and associated with a contourite drift and a slope break. The main difference is that contourite channels are dominated by erosion, with clearly truncated reflections at the drift. Moats are not always purely erosional features and their formation and evolution is often also influenced by deposition and winnowing (Miramontes et al., 2021; Wilckens et al., 2023a).

Due to the effect of the Coriolis force, contourite drifts are found either on the right side of the moat (southern hemisphere) or on the left side (northern hemisphere), with a view in the downstream direction of the bottom current (Faugères et al., 1999; Rebesco et al., 2014). The development, morphology, and internal architecture of moat-drift systems are controlled by slope angle, current velocity, and sediment supply (Wilckens et al., 2023a,b).

Moats and paleo-moats are useful for bottom current reconstructions, serving as current intensity and direction indicators. Recent studies have proposed further classifications based on seismic reflection patterns and the spatial location of moats found on the seafloor (Betzler et al., 2014; Wilckens et al., 2023a). Hence, moats are classified into three types: i) Constructional moats are the most dominant type, which have been observed and reported worldwide, having the ability to migrate upslope and exhibiting an aggrading stacking pattern with deposition at the moat bottom and the drift (Wilckens et al., 2023a). ii) Mixed depositional-erosive moats show an equilibrium between erosion and deposition, with lateral migration and vertical stacking. iii) Erosional moats are identified by non-deposition at the bottom of the moat and eroded drift flanks. They can be distinguished by differences in width, height, and angle with respect to drift crest, moat thalweg, and slope (Wilckens et al., 2023a). The depositional part of the system is characterized by drifts that develop under relatively slow-flowing bottom-currents and accumulate from suspension-transported sediments. Hence, they form over a long period of time, recording changes in water-mass properties and bottom-current velocities (Faugères et al., 1999; Hernández-Molina et al., 2022). Contourite drifts are classified based on the degree of mounding and progradation and have been described for numerous continental margins. The contourite deposits at the Argentine Continental Margin (ACM), as well as their variations, have been the target of scientific research over the last years (Franke et al., 2007; Preu et al., 2012; Gruetzner et al., 2012, 2016; Miramontes et al., 2016; Steinmann et al., 2020; Wilckens et al., 2021, 2023a; Warnke et al., 2023). Until now, no record of the presence and evolution of moat-drift systems in the Tertiary has been reported for the Argentine margin, and moat parameters and classifications are restricted to constructional- and erosional moat observations from the seafloor. This study focuses on applying moat-drift system classifications to decode a complex buried moat-drift system at the Argentine margin to decipher the extension and intensity of bottom-currents, as well as their evolution between the Early

Oligocene and the Early-to-Middle Miocene. Here, we focus on buried moat-drift systems of the Southern Ewing Terrace (SET) made visible with newly acquired high-resolution seismic profiles.

Geological setting and morphological context

The area of interest is located at the Argentine Continental Margin, which is part of the rifted volcanic continental margin east of South America (Fig. 1; Hinz et al., 1999; Franke et al., 2007). The rifting processes favored the development of several transfer fracture zones and the formation of E-W and NW-SE trending sedimentary basins (Franke et al., 2007). At the Eocene-Oligocene boundary, the opening of the Drake Passage and the initial expansion of the Antarctic ice sheet mark the beginning of the thermohaline circulation in the South Atlantic, which would eventually shape a large CDS along the entire Argentine margin (Hernández-Molina et al., 2009; Preu et al., 2013; Ercilla et al., 2019). As part of the CDS, numerous erosional and depositional contourite features developed, like contourite terraces, contourite drifts, contourite channels, and moats. In the study area, the slope of the ACM is dominated by a step-like morphology, exhibiting three contourite terraces, which are separated by either a steep erosional surface, a moat, or both (Preu et al., 2013). These are from the upper to lower slope, the La Plata Terrace (500-600 m), the Ewing Terrace (1100-1500 m; Fig. 1B), and the Necochea Terrace (>3500 m). The Mar del Plata (MdP) Canyon separates the Ewing Terrace into Northern Ewing Terrace (NET) and Southern Ewing Terrace (SET) (Preu et al., 2012; Voigt et al., 2013; Warratz et al., 2019).
Changes in the depositional environment at the Ewing Terrace are expressed in contourite deposit variations. While the SET is limited in width by the upslope presence of ET-Moat 1, which extends along the middle slope (Fig. 1; 1000-1300 m, 96 km long, 7 km wide and 100 m deep; Steinmann et al., 2020; Bozzano et al., 2021; Wilckens et al., 2023a), the NET is wider (Fig. 1) and upslope delimited by a different moat in shallower water depths (ET-Moat 2; 700-850 m water depth). ET-Moat 2 is, in contrast, shorter, wider, and deeper than ET-Moat 1. Both terrace sections are basinward, characterized by a drift, which developed a mounded drift crest at the SET but is less pronounced at the NET (Fig. 1; Preu et al., 2013; Wilckens et al., 2021).

Modern oceanographic setting

The Argentine margin is an exceptional key region since it is the only location in the Southern Ocean where counterflowing polar and tropical water masses meet and exchange (Piola and Matano, 2019) (Fig. 1A). Regional circulation is characterized by surface, intermediate and deep-water masses (Piola and Gordon, 1989; Stramma and England, 1999). The northward flowing Malvinas Current (MC) originates from the Antarctic Circumpolar Current (ACC), thus being a cold subpolar nutrient-rich water with contributions from the Sub Antarctic Water (SAW; < 500 m), the Antarctic Intermediate Water (AAIW; 500-1200 m) and the Upper Circumpolar Deep Water (UCDW; 1200-1700 m). The barotropic MC flows along the Patagonian shelf and slope before meeting the southward-flowing Brazil Current (BC) (Fig. 1C; Artana et al., 2021). Within the upper 500 m, the BC flows southward along the Brazilian shelf, including components of Tropical Water (TW) and South Atlantic Central Water (SACW) (Piola and Matano, 2019). The warm, nutrient-poor, but saline BC encounters the MC at around 38-39° S, forming the Brazil-Malvinas Confluence (BMC) zone (Gordon, 1989). Within the vicinity of the BMC zone, the MC splits into three branches at the seafloor. MC-1 follows the upper slope at the La Plata Terrace, while MC-2 flows along the interface of La Plata- and Ewing Terrace and the third branch (MC-3) flows basinward of the Ewing Terrace (Fig. 1C; Wilckens et al., 2021). Furthermore, the BMC zone exhibits a strong front that meanders in mean flow and vertical eddies, showing a severe mesoscale variability (Berden et al., 2020). The northward-flowing AAIW and the Upper Circumpolar Deep Water (UCDW) dominate the intermediate circulation. The UCDW and Lower Circumpolar Deep Water (LCDW) are separated by the intrusion of the relatively warm and saline southward-flowing North Atlantic Deep Water (NADW) before it steers eastward into the Argentine Basin (Fig. 1C; Piola and Matano, 2019). The NADW flowing at depths of 1500-2800 m, touches the slope north of the MdP Canyon but separates from the seafloor south of the MdP Canyon (Arhan et al., 2002; Preu et al., 2012). Deep water circulation (>3500 m water depth) is dominated by the Antarctic Bottom Water (AABW), which introduces cold and oxygen-rich waters from the Antarctic to the Argentine Basin (Piola and Matano, 2019).

Regional seismostratigraphy and paleoceanography

Numerous seismostratigraphic models previously proposed have tried to connect deposits along the Argentine continental margin with paleotectonic and -oceanographic events (Ewing and Lonardi, 1971; Urien and Zambrano, 1973; Hinz et al., 1999; Franke et al., 2007; Hernández-Molina et al., 2009, 2010; Violante et al., 2010; Preu et al., 2012; Gruetzner et al., 2012, 2016; Loegering et al., 2013; Ercilla et al., 2019; Rodrigues et al., 2020; Kirby et al., 2021; Rodrigues et al., 2022). Some of these models are ground-truthed by industrial wells (Fig.1A), located near the shelf (Ewing and Lonardi, 1971; Violante et al., 2010; Kirby et al., 2021). Hence, most of the available age models are derived from seismostratigraphic correlation between comparable unconformities and seismic units recognized throughout the area.

Regional unconformities of interest for this study are AR3 (Paleocene/Eocene boundary, ~56 Ma, Fig. 2), AR4 (Eocene/Oligocene boundary, ~34 Ma), AR5 (Early/Middle Miocene, ~16 Ma), AR6 (Middle Miocene, ~14 Ma), AR7 (Late Miocene, ~6 Ma) and AR8 (Pleistocene/Holocene boundary, ~1.8 Ma) (Fig. 2 and Fig. 3). AR4 and AR5 are prominent reflectors that can be found not only at the SET (Gruetzner et al., 2016; Violante et al., 2010) but were also described by Preu et al. (2012) at the NET and thus indicate a similar paleoceanographic evolution along the Ewing Terrace. Deposits (and their bounding unconformities) younger than AR5 can only be correlated by the seismic facies since the MdP Canyon disrupts the reflectors. Several Seismic Units (SU1-7; Fig. 2) have been described in the subsurface of the SET according to their unconformities. There is, however, a controversy about the seismic units and their exact ages. Thus, the presented units in this study show a compilation of four studies (Violante et al., 2010; Preu et al., 2012; Gruetzner et al., 2016; Ercilla et al., 2019). The oldest unit (SU1) is located beneath the feature of interest and is therefore omitted from this study. SU2 is the lowermost identified unit and is characterized by wedge-shaped upslope migrating plastered drifts that developed by the formation of a circulation system that was reinforced by gradual seafloor deepening and widening of the South Atlantic Ocean, leading to the introduction of Upper Pacific Waters (UPW) into the ACM (Fig. 3; Uenzelmann-Neben et al., 2017; Batenburg et al., 2018). SU3 is dominated by weak to medium acoustic responses and a bank-like morphology developed during the initiation of the ACC. The introduction of ACC led to MC branches to the ACM by the opening of the Drake Passage (Preu et al., 2012; Ercilla et al., 2019). During the deposition of SU4, the BMC zone had presumably a similar position as today, followed by a change of deposition to wide plastered drifts associated with the widening of the Drake Passage and the subsequent strengthening of the circumpolar circulation (Kennett et al., 1985), accompanied by the rearrangement of the water masses as well as the initial separation of CDW into LCDW and UCDW. After the Mid-Miocene Climatic Optimum (MMCO) and the Antarctic ice-sheet expansion, sea level decreased, resulting in the deposition of SU5 and its sub-units, which show that the remaining depocenter is found landward with aggregational sequences while the sediments deposited facing the sea experienced extensive reworking and erosion (Fig. 2; Gruetzner et al., 2011; Preu et al., 2012; Ercilla et al., 2019). The youngest sequences (SU 6-7) are associated with a strengthening of the bottom-currents between late Miocene to early Pliocene and finally the closing of the Central American Seaway (CAS) along with an increase of NADW flux, which resulted in the development of terraces and the deposition of plastered drifts (Fig. 3; Preu et al., 2012; Ercilla et al., 2019). SU7 is only partially displayed and is not the focus of the study. The main focus relies on SU3 and the buried moat-drift systems within.

DATASET AND METHODS

Bathymetric data

The regional bathymetry used in this study corresponds to GEBCO 2023 (Fig. 1; GEBCO Compilation Group, 2023). Additionally, multibeam bathymetry of the study area was collected during research cruises SO260 with RV SONNE in 2018 (Kasten et al., 2019), as well as expeditions, M78-3 (2009; Krastel and Wefer, 2011) and M49-2 (2001; Spiess et al., 2002) with RV Meteor (Fig. 1B). The hull-mounted Kongsberg EM122 aboard SONNE operates with a frequency of 12 kHz and an opening angle of 150°, which results in a beam footprint of 0.5° x 1°. On Meteor, the hull-mounted Kongsberg EM120 has a beam footprint of 1° x 2° with the same frequency and opening angle as the EM122. The data was processed with the open-source MB-System software (Caress and Chayes, 1996) and quality checked with Fledermaus. For visualization, the grids with a resolution of 25 m (SO260) and 50 m (M78-3 and M49-2) were imported into the open-source geographic information system QGIS.

Seismic reflection data

The seismic data shown in this study was collected during expedition SO260, and the acquisition was made with the high-resolution multichannel seismic system from the University of Bremen, which includes a SERCEL Mini GI-Gun with 0.24 l volume for the generator and injector and a SERCEL GI Gun with 0.4 l volume for the generator and injector. Both sources emit sound waves with a maximum frequency of 250 Hz, leading to a maximum vertical resolution of 1.6 m. A 250 m long TELEDYNE streamer with 96 channels, hosting four sections with varying channel spacings from 1 to 4 m, was towed in 1 m water depth and controlled by four ION DigiBirds. A total of 174 km of multichannel seismic data were collected from which 155 km were processed and analyzed for this study.

The data signal was recorded and digitized with MaMuCS (Marine Multi-Channel Seismic Acquisition System), a custom-designed software developed at the Marine Technologies/Environmental Research Working Group at the Faculty of Geoscience at the University of Bremen. The sampling rate was set to 0.25 ms, and the recording length was set to 3 or 6 s with respect to the water depth and signal penetration. All shown seismic profiles underwent the same processing workflow, including band-pass filtering (10/30/800/1600), an interactive velocity analysis followed by a normal moveout (NMO) correction, static correction, noise removal (THOR, 2D-Despike, 4D-Dec) and finally a migration. Processing of the seismic data was conducted using *VISTA 2016 seismic data processing software* (Schlumberger), while interpretation was realized with *The Kingdom Software 2019* (IHS). Processed, uninterpreted images of the seismic profiles used in the present study are provided in the supplementary materials (Figs. SU1-SU3).

Seismic Nomenclature

Based on multichannel reflection seismic and thus the interpretation of reflection terminations, a seismic facies description was carried out, using terminology outlined by Mitchum et al. (1977), Faugères et al. (1999) and Rebesco and Stow (2001). Seismic facies and unconformities therein are used to determine depositional and erosional events and associated structures. Contourites can be identified over different spatial scales. First-order deposits are distinguishable over geometry and spatial extents, secondary-order features display minor variations and discontinuities, while third-order features show the highest resolution with small features based on their internal seismic facies and reflection terminations (< 1 km; Rebesco et al., 2014).

The criteria used for identifying buried moat-drift systems is based on Rebesco et al. (2005, 2014) and Wilckens et al. (2023a), and therefore, in this study, the reflection terminations of a drift define the moat classification. Hence, a constructional moat describes a seismic reflection pattern that follows the moat morphology and onlaps on the slope side. A mixed moat, on the contrary, shows increased seismic amplitudes with continuous seismic reflections from drift to moat angle, thus, the reflections downlap on the bottom of the moat. The deepest point of the moat is termed a moat thalweg (sometimes also referred to as trough), and the shallowest part of a moat-drift system is a drift crest (Wilckens et al., 2023a). Above, the shape of the moat thalweg and the migration direction of moat-drift systems can either be a flat shape or a concave-up shape (Wilckens et al., 2023a; Zhao et al., 2024). And lastly, an erosional moat is characterized by truncated reflections towards the moat thalweg (Wilckens et al., 2023a). Based on the above-mentioned classification the criteria for recognizing moats include: 1) reflection truncation, 2) relationship with drift accumulations, and 3) the slope angle between drift and moat. Height and width of the moats and drifts are calculated assuming a constant velocity of 1500 m/s; therefore 1 s TWT corresponds to 750 m.

RESULTS

Seismostratigraphy of the buried moat-drift systems

Since the main focus of the study are buried moat-drift systems, the seismic analysis targets only a specific area of the SET (Fig. 4). Four seismic profiles were selected to demonstrate variations along the SET from North (GeoB18-36; Figs. 5, S2) to the Center (GeoB18-38 and -32; Figs. 6A, S2, 6C, S3) and finally to the South (GeoB18-73; Figs. 7, S3), with distances between each profile of at least 9 km (Figs. 1B, 4) and a maximum distance between the southern and northern profile of 74 km. Additionally, SU3 (Figs. 2, 3) will be described in detail in these sections as this is the unit of interest for this study.

SU3 is a dominant unit at the SET that can be identified throughout the area. In general, this unit illustrates reflections with a wide range of amplitudes but is easily recognizable by the complex internal stacking pattern, which hosts high-amplitude reflectors that are accompanied by local low-amplitude chaotic facies (Fig. 2). In addition, the distinct erosional unconformity at the base (AR4; Fig. 2) is characterized by a high-amplitude reflection. Furthermore, several cut-and-fill structures and mounded-shaped, semi-continuous to discontinuous reflections can be discerned, making this unit very heterogeneous regarding the lateral and spatial appearance. The thickness of SU3 reaches up to 490 m in the northeastern sector (Fig. 4; GeoB18-036, close to the MdP Canyon) and is thinnest in the southern sector (GeoB18-073), with only 150 m of thickness beneath the present-day drift crest. Therefore, the unit increases in thickness towards the North (Fig. 4). The base of SU3 corresponds to Reflector AR4 derived from Violante et al. (2010), Preu et al. (2012) and Gruetzner et al. (2016). AR4 is found in depths of 1700 m to 2400 m (Fig. 4), with the shallowest depth in the western part of the study area (outside of the shown seismic sections) and the deepest depths (2400 m) in the eastern part of the study area. AR4 exhibits a step-like appearance, with an NNE-SSW orientation incorporating a sharp depth drop, decreasing from 1600 m to 2100 m within 10 km (Fig. 4). At the top SU3 is limited by the erosive discontinuity AR5, which is present in depths between 1350 m and 1900 m (Fig. 2).

Subsurface structures and geomorphology of the moat-drift architecture

SU3 increases in thickness from south to north and reaches a maximum of 490 m (Fig. 5). Low-amplitude reflections and chaotic facies dominate the stacking pattern close to AR4, on which the buried moat-drift systems developed and reveal eight alternating cycles; each cycle is represented by the development of a moat-drift system. The alternating cycles can be distinguished by narrow distances from drift crest to slope and furthermore exhibit the steepest and largest observed drift flanks compared to the other seismic profiles (Fig. 5A).

Eight moat-drift systems (M-D1-8) can be identified in the northern sector of the SET (e.g. Fig.5) at depths of ~300 mbsf. Each M-D system depicts individual geometric properties and reflection amplitudes (high-low; Fig. 5). Four of the structures are erosionally truncated and do not terminate against AR4 (M-D1, 2, 4 and 5; < offset 32km) but are overlain by younger M-D systems. The younger deposits (M-D3, 6-8) are constructional moats with a flat shape and steep flanks (2.1–2.5 s TWT, 26–30.5 km offset). The separated mounded drifts reach heights between 150-750 m and widths of 1-2.5 km. The low-amplitude reflections downlap onto the transparent amplitude zone and restrict moat-drift geometry identifications of the systems (Fig. 5). For M-D1, -4, and -5, the drift crests were not distinguishable. On top of that, the medium amplitude reflections are erosionally truncated by younger M-D systems and show only a limited amount of mounding character. Nevertheless, it was possible to measure geometries for M-D2 and -3, which are located in the center of SU3 (offset 31-34.5 km and 2.4-2.6 s TWT; Fig. 5B). With a width of 6.8 km and a relief of 157.5 m M-D2 reveals erosional moat characteristics since the reflections (of medium amplitude) are erosional truncated (Fig. 5). The adjacent younger system (M-D3) has a relief of 112.5 m and a width of 4 km (Fig. 5B). This constructional moat has a flat shape and is delimited by M-D5 and -6. Both moat-drift systems (M-D 2 and -3) are unique and only found in this part of the study area. The above-lying M-D systems (M-D 6-8) show a higher degree of mounding, and while the drift crests are well-developed, the moat thalwegs and the slope distances are not clearly identifiable, as these are masked and distorted by the low-amplitude zone which does not allow for accurate measurements (Fig. 5A).

In the central northern part of the SET (e.g. Fig. 6), the thickness of unit SU3 is 400m thick (Fig. 4B). Here, SU3 displays low- to medium amplitude reflections and a wavy stacking pattern in the lower part of the section (> 2.45 s TWT; Fig. 6A), whereas the upper part is dominated by continuous medium- to high amplitude reflections, occasionally disrupted low-amplitude and chaotic reflections. Three M-D systems (M-D1-3; Fig. 6A, C) can be identified in depths of ~487.5-712.5 mbsf within SU3. Again, AR4 marks the base on which the three M-D systems terminate (M-D 1-3, Fig. 6B, D). All three M-D systems show a characteristic constructional moat morphology with a concave-up shape and mounded geometries of the associated drifts. The range of width between the drift crest and slope ranges between 0.7 and 2.4 km in this part of the study area, representing the minimum width value observed. The relief extends from 22.5 to 37.5 m. Notable are the low-amplitude to transparent seismic reflections found in the moat thalwegs (Fig. 6A, C). While the smallest relief parameters are found within this area, the slope angle is the steepest (> 3°; Fig. 6A and Fig. 8E), which can only be observed in the northern and southern sections of the study area. M-D2 can be found in depths of ~637.5 mbsf and shows only minor variations in this area, where the width varies by 1 km and the relief by approximately 10m (Fig. 6B).

The southernmost sector of the SET (Fig. 7) shows the internal stacking pattern of SU3, which exhibits a complex sigmoid-oblique pattern with a few isolated high-amplitude reflections (Fig. 7A). At around 2.4 s TWT and offset 16.5 km, a constructional moat with a width of 3.75 km and a relief of 135 m can be recognized (Fig. 7B). This moat displays a concave-up shape morphology that migrates upslope in depths of 600-675 mbsf. The depth below seafloor at which the buried M-D1 can be found (Fig. 7) corresponds to the depth at which M-D3 from the central sections can be identified (Fig. 6). With decreasing slope angle, found in the upper part of SU3 we notice the disappearance of moat-drift systems.

In summary, the buried moat-drift systems display a wide range of appearances, and some correlation from system to system is only possible in the central area, whereas the systems in the northern and southern areas differ significantly. Additionally, the relief displays a deepening from south to north, associated with increasing M-D systems from one system to approximately eight systems (157-13.5m; M-D1-8; Figs. 5-8). The identified moat-drift systems exhibit a strong dominance of constructional moats with a concave shape (Figs. 6, 7). Only one erosional moat and one constructional moat with a flat shape were identified (Fig. 5)

DISCUSSION

Morphosedimentary analysis of the paleo-moat-drift deposits

The paleo-moat-drifts identified along the SET, in depths of ~400-712 mbsf, are located in seismic unit SU3 and are bounded at the bottom by the stratigraphic marker that represents the Eocene-Oligocene boundary (Figs. 5-7). The upper limit of SU3 is the stratigraphic marker of the Early to Middle Miocene age (AR5), which marks the disappearance of the paleo-moat-drift systems indicated by the change in seismic characteristics and by the shift from being erosional contourites to only depositional contourites.

The buried moat-drift systems of the SET generally display a series of constructional moats (Figs. 5, 6) with upslope migrating behavior. Notably, the northern sector of the SET shows a clear increase in the abundance and density of M-D systems. The buried moat-drift systems can be clearly identified along the SET, displaying a series of constructional moats (Figs. 5, 6). Nevertheless, these high-frequency changes in moat-drift deposition, accompanied by changes in drift crest formation and steep drift angle, can only be found in this part of the study area (Fig. 8). Constructional moats with a concave-up shape dominate SU3, and only one constructional moat with a flat base (M-D7) and one erosional moat with a concave-up shape (M-D5) were identified within this seismic unit. This supports the assumption that several moat types can develop and migrate within a unit without being restricted to one type. The formation, migration, and internal structure of the observed M-D systems in the study area would suggest increased current speed and decreasing sediment availability from the South to the North. Increasing current velocity, accompanied by more erosion is present and less deposition, restricts the build-up of large and well-established drifts close to the paleo-moats. Nevertheless, the identified moat-drift systems can be compared to the modern moat-drift systems already described at the Argentine Margin (Ewing Terrace Moat 1 and -2; Steinmann et al., 2020; Wilckens et al., 2021), the Mozambique Margin (Beira Moat; Thiéblemont et al., 2019; Miramontes et al., 2021; Wilckens et al., 2023a) and the Spanish Margin (Álvarez Cabral Moat and Gijón Moat; Hernández-Molina et al., 2015; Liu et al., 2020). Between the observed buried erosional moat and the Álvarez Cabral Moat, are similarities in internal structure, but relief and width differ, which may be due to the fact that the moat in the South of Spain is still actively shaped. The buried moat-drift system in SU3 was most likely affected by secondary processes, like erosion and reworking. The buried constructional moats in our study area are also comparable to the Gijón Moat or the Beira Moat, although with smaller reliefs and width than the mentioned moat-drift systems.

Moat-drift architecture and associated current dynamics

Within the buried moat-drift systems at the SET, an interdependence of relief and width revealed clusters based on the locations; thus two clusters of M-D systems can be distinguished according to their dimensions (Fig. 8A). Therefore, the greater the width, the higher the relief, which can be found in the northern and southern areas. Whereas, the central sector of the SET presents smaller widths and reliefs (Fig. 8A). While the slope angle varies by around 3° at AR4, a relationship between steep slope angle and drift angle is not evident for the identified M-D systems in our study area, thus indicating no correlation over the entire area (Fig. 8E). However, if only the central area of the SET is considered, a correlation can be recognized (Fig. 8E).

It has been suggested that steep slopes and fast currents lead to steep drift flanks and thus paleo-moat morphology can be used as an indicator for paleo-velocity estimations (Wilckens et al., 2023b). Based on the seismic data, the internal structure of the moat-drift systems in the northern sector reveals alternations from slower to faster current flow velocities with medium to high drift angles. In general, the slope angle is within the range of 2° to 3.1° over the entire area, pointing to a variation of slope angle of 1.1° (Fig. 4), which together with no apparent morphological changes indicates conditions that favor uniform current velocities over the paleomargin (Figs. 3, 8F, 9). No clear trend between the northern, central, and southern parts of the study area is definite; thus secondary processes such as erosion have to be considered, which not only alter moat-drift dimensions but also bias correlations (Fig. 8C). One M-D system stands out with an exceptionally high slope angle (M-D 038-3; Fig. 8F), but against the assumption that the drift angle should also be high, the M-D system illustrates median values for the drift angle. Besides this system, the M-D systems identified at the northern and southern parts of the study area display the greatest drift angles despite having an average slope angle (~ 2.7°; Fig. 8). Hence, the slope angle is not the only key function, but the sediment availability, current velocity, and the erosive power are the final contributors when establishing steep drift flanks and drift geometries. Therefore, the identified M-D systems are most likely the result of a local bottom current influence which resulted in a high drift angle. Other identified M-D systems in the central part display a relatively homogenous internal structure, indicating steady current velocities that remain stable over the central part of the terrace (Fig. 9). The observed contourite drifts present isolated high-amplitude reflections interbedded in low-amplitude reflections (Fig. 5 and Fig. 9), which commonly indicate variations in the grain size related to oscillations in the bottom current-velocity (Llave et al., 2016; Miramontes et al., 2016, 2019). Additionally, the upslope migrating behavior and internal structure of constructional moats indicate moderate to high current velocities and relatively high sediment availability (Wilckens et al., 2023a). High-frequency changes of buried moat-drift location with an erosional moat are evident for the northern part of the study area. Local waxing and waning of bottom-currents was previously reported for the SD-S (Fig. 1B; Warnke et al., 2023) where the shifting of bottom-currents in space but also variations in intensity caused numerous clinoforms. Here, two processes seem reasonable for the formation of the northernmost M-D systems: 1) One possible process that initiated the waxing and waning of the currents in the northern section could be related to the onset of the MdP Canyon. How and when the MdP Canyon developed is not fully understood. It is assumed that the MdP Canyon was established during the Late Miocene, but it cannot be ruled out that shaping processes impacted the area before the Late Miocene (Preu et al., 2012). Therefore, it is possible that the onset of the canyon may have impacted the along-slope processes forming both the erosional and depositional contourite features, and shifted the main depocenter in stages to the East.

Depending on the bottom current strength, the depocenter eventually shifted to the West again, and the increase of current strength becomes evident with the finding of an erosional moat. 2) Another reasonable process that led to the formation differences of the moat-drift systems along AR4 could be related to downslope processes. Transparent zones at the foot of the paleo-moats and the absence of terminations against AR4 indicate that the moats are filled with mass transport deposits (Figs. 5-7). The filling supports the upslope movement of the moats. Similar transparent zones at the foot of paleo-moats can be found in the central profiles (Fig. 6) but are not as apparent in the southern sector. In the case of mass transport processes, the slope angles can be altered, changing moat-drift geometries. Downslope processes like mass transport deposits have already been verified in the MdP Canyon and at the lower slope of the Argentine margin (Voigt et al., 2013; Gruetzner et al., 2016; Warratz et al., 2019). The eastward shift, together with increased bottom current velocities, resulted in the development of the steep drift flanks found in M-D2 and -3. These observations can be linked to an enhancement of bottom current velocity reaching a maximum towards the North, which would explain why the most complex moat-drift deposits are found in the northernmost profile (Figs. 5, 7).

In the final stage, the upslope migrating paleo-moats reached a very low slope angle (<1°; Fig. 2), marking the offset of the moat-drift deposits. Being no longer morphologically restricted, the bottom current broadened, and the deposition of plastered drifts in SU4 began (Fig. 9; Wilckens et al., 2021).

Paleoceanographic and -tectonic impact during Oligocene to Early-Middle Miocene

The northernmost area of the SET represents the area with more erosional events and indicates the highest variability of bottom current activity and intensity. Previous studies have suggested that the introduction of deep-water circulation initiated with the opening of the Drake Passage and, therefore the introduction of the ACC allowed the onset of the highly complex oceanography that can still be found at the ACM today (Hinz et al., 1999; Hernández-Molina et al., 2009; Preu et al., 2012). With respect to the paleoceanography and -climate during the Oligocene, the opening of the Drake Passage, together with a generally cooler climate, resulted in the thermal isolation of Antarctica and also in a strengthening of the MC being a branch of the ACC (Peterson and Stramma, 1991; Katz et al., 2011). These processes led to the formation of the erosional unconformity AR4, which can be found along the entire Argentine margin. The development of a steep slope during this time established the foundation for the onset of the moat-drift systems in our study area (Fig. 9). During the following 22 Ma, current velocity and current depth changes in the regional current system resulted in the deposition of several moat-drift systems. The initiation of the MC at the ACM resulted in the development of a proto-BMC zone, and with that, gradual strengthening and sea level rise resulted in an upslope migration. Based on the development of mounded drifts on the right side of the observed moats, a northward flowing current is proposed, regulated by erosion in the west and deposition in the east (Fig. 9; Faugères et al. 1999) was operating during the deposition of SU3 (Early Oligocene to Middle Miocene). It is known that the BMC zone today is a highly dynamic oceanographic system whose position varies seasonally but also annually depending on wind forcing and temperature (Artana et al., 2019; Wilckens et al., 2021; Alonso et al., 2023). Therefore, it can be assumed that the complex paleoceanographic dynamic already developed during the Oligocene and influenced the deposition on a regional scale, reflecting climatic changes onto shifts at the confluence zone. The progressive opening of the Drake Passage by continental stretching and oceanic spreading resulted in sea level rise, and current strengthening that continued to form and modify the depositional sequences (Fig. 9). In the late Miocene, slower oceanographic dynamics prevented further formation of moat-drift systems.

CONCLUSIONS

In this study, we used high-resolution seismic profiles acquired during R/V SONNE cruise SO260 to reveal for the first time the spatial and vertical distribution of a buried-moat-drift sequence during the Early Oligocene to the Middle Miocene. This finding suggests that the complex oceanographic setting had an onset at around 34 Ma and lasted approximately until 18 Ma. The buried moat-drift system built up along the NE-SW-oriented escarpment formed at the Argentine Margin during the Eocene to Oligocene boundary by the regional discontinuity AR4. The drift deposition on the eastern side of the moat suggests a northward flowing current along the slope. With the opening of the Drake Passage, the Malvinas Current progressively entered the Argentine continental margin, and together with the southward flowing currents, the Brazil-Malvinas Confluence (BMC) zone started to establish. It is known that the BMC zone has seasonal to annual changes in location. The high variability of the moat-drift systems in the northern part of the study area is interpreted to be the result of a shifting BMC zone. Therefore, it can be hypothesized that the BMC zone was unstable in location since the Oligocene. The upslope migrating behavior and the establishment of constructional moats point to high bottom current velocities with limited sediment availability, while the erosional moat argues for even stronger bottom-currents with low sediment availability. Additionally, the findings of this study reveal for the first time, multiple M-D systems that can migrate within a sedimentary unit and are not limited to one moat-drift type. With the widening of the Drake Passage and the absence of a steep slope, the bottom current broadened along the margin, leading to the termination of buried moat-drift systems in the Miocene. Our study highlights the importance of high-resolution seismic imaging for identifying paleo-moats that would remain undiscovered. The exceptional paleo-moats underline the complexity of the CDS at the Argentine Margin and are a clear indicator of the onset of dynamic oceanographic conditions.

ACKNOWLEDGMENTS

We thank the nautical crew and onboard scientific teams for their work during cruise *SO260* onboard *R/V SONNE 2018*. Expedition *SO260* was funded and carried out in the framework of the Research Centre/Cluster of Excellence ‘The Ocean in the Earth System’ (MARUM – Center for Marine Environmental Sciences at the University of Bremen). We acknowledge additional funding from the Helmholtz Association (Alfred Wegener Institute Helmholtz Centre for Polar and Marine Research, Bremerhaven). Schlumberger (VISTA 2D/3D Seismic Data Processing) and IHS Global Inc. (Kingdom Software) generously provided academic software licenses. We thank Lena Steinmann, Rouven Brune and Fynn Warnke for processing the multibeam bathymetry data from the Ewing Terrace. Insightful comments and suggestions by G. Pantopoulos, one anonymous reviewer, the corresponding editor, J. B. Southard, and guest editor, G. Postma, greatly helped to improve this manuscript.

DATA AVAILABILITY STATEMENT

The raw multibeam EM122 data of RV SONNE cruise SO260/1 is available at the PANGAEA Data Publisher *via* https://doi.pangaea.de/10.1594/PANGAEA.888569.

DECLARATION OF COMPETING INTEREST

The authors declare that they have no known competing financial interests or personal relationships that could have appeared to influence the work reported in this paper.

REFERENCES

Alonso, J.J., Vidal, J.M., and Blázquez, E., 2023, Why Are the High Frequency Structures of the Sea Surface Temperature in the Brazil–Malvinas Confluence Area Difficult to Predict? An Explanation Based on Multiscale Imagery and Fractal Geometry: Journal of Marine Science and Engineering, v. 11, no. 1096.

Arhan, M., Naveira Garabato, A.C., Heywood, K.J., and Stevens, D.P., 2002, The Antarctic Circumpolar Current between the Falkland Islands and South Georgia: Journal of Physical Oceanography, v. 32, pp. 1914–1931.

Artana, C., Provost, C., Poli, L., Ferrari, R., and Lellouche, J.-M., 2021, Revisiting the Malvinas Current Upper Circulation and Water Masses Using a High-Resolution Ocean Reanalysis: Journal of Geophysical Research, v. 126 (6) e2021JC017271

Artana, C., Provost, C., Lellouche, J.-M., Rio, M.H., Ferrari, R., and Sennéchael, N., 2019, The Malvinas Current at the Confluence With the Brazil Current: Inferences From 25 Years of Mercator Ocean Reanalysis: Journal of Geophysical Research, v. 124, pp. 7178–7200.

Batenburg, S.J., Voigt, S., Friedrich, O., Osborne, A.H., Bornemann, A., Klein, T., Pérez-Díaz, L., and Frank, M., 2018, Major intensification of Atlantic overturning circulation at the onset of Paleogene greenhouse warmth: Nature Communications, v. 9, no. 4954.

Berden, G., Charo, M., Möller O.O.Jr., and Piola, A.R., 2020, Circulation and Hydrography in the Western South Atlantic Shelf and Export to the Deep Adjacent Ocean: 30°S to 40°S: Journal of Geophysical Research, v. 125 (10) e2020JC016500.

Betzler, C., Lindhorst, S., Eberli, G.P., Lüdmann, T., Möbius, J., Ludwig, J., Schutter, I., Wunsch, M., Reijmer, J.J.G., and Hübscher, C., 2014, Periplatform drift: The combined result of contour current and off-bank transport along carbonate platforms: Geology, v. 42, pp. 871–874.

Bozzano, G., Cerredo, M.E., Remesal, M., Steinmann, L., Hanebuth, T.J.J., Schwenk, T., Baqués, M., Hebbeln, D., Spoltore, D., Silvestri, O., Acevedo, R. D., Spiess, V., Violante, R., and Kasten, S. 2021, Dropstones in the Mar del Plata Canyon Area (SW Atlantic): Evidence for Provenance, Transport, Distribution, and Oceanographic Implications: Geochemistry, Geophysics, Geosystems, v. 22 (1) e2020GC009333.

Caress, D.W., and Chayes, D.N., 1996, Improved processing of Hydrosweep DS multibeam data on the R/V Maurice Ewing.: Marine Geophysical Researches, v. 18, pp. 631–650.

Dorschel, B., Hehemann, L., Viquerat, S., Warnke, F., Dreutter, S., Schulze Tenberge, Y., Accetella, D., An, L., Barrios, F., Bazhenova, E.A., Black, J., Bohoyo, F., Davey, C., de Santis, L., Escutia, D., Carlota Fremand, A.C., Fretwell, P.T., Gales, J.A., Gao, J., Gasperini, L., Greenbaum, J.S., Henderson Jencks, J., Hogan, K.A., Hong, J. K., Jakobsson, M., Jensen, L., Kool, J., Larin, S., Larter, R.D., Leitchenkov, G L., Loubrieu, B., Mackay, K., Mayer, L., Millan, R., Morlighem, M., Navidad, F., Nitsche, F.O., Purser, A., Rebesco, M., Rignot, E., Roberts, J.L., Rovere, M., Ryzhov, I., Sauli, C., Schmitt, T., Silvano, A., Smith, J.E., Snaith, H., Tate, A.J., Tinto, K., Vandenbossche, P., Weatherall, P., Winterstellar, P., Yang, C., Zhang, T., and Arndt, J.E., 2022, The International Bathymetric Chart of the Southern Ocean Version 2 (IBCSO v2), Scientific Data (9).

Ercilla, G., Schwenk, T., Bozzano, G., Spiess, V., Violante, R.A., Estrada, F., Ianniccheri, F., Spoltore, D.V., and Alonso, B., 2019, Cenozoic sedimentary history of the northern Argentine continental slope, off Bahia Blanca, the location of the Ewing Terrace: Palaeogeodynamic and palaeoceanographic implications: Marine Geology, v. 417, 106028.

Ewing, M., and Lonardi, A.G., 1971, Sediment transport and distribution in the Argentine Basin. 5. Sedimentary structure of the Argentine margin, basin, and related provinces: Physics and Chemistry of The Earth, v. 8, pp. 125–251.

Faugères, J.-C., Stow, D.A.V., Imbert, P., and Viana, A., 1999, Seismic features diagnostic of contourite drifts: Marine Geology, v. 126, pp. 1–38.

Franke, D., Neben, S., Ladage, S., Schreckenberger, B., and Hinz, K., 2007, Margin segmentation and volcano-tectonic architecture along the volcanic margin off Argentina/Uruguay, south Atlantic: Marine Geology, v. 244, pp. 46–67.

García, M., Hernandéz-Molina, F.J., Llave, E., Stow, D.A.V., León, R., Fernández-Puga, M.C., del Rio, V.D., and Somoza, L., 2009, Contourite erosive features caused by the Mediterranean Outflow Water in the Gulf of Cadiz: Quaternary tectonic and oceanographic implications: Marine Geology, v. 257, pp. 24–40.

General Bathymetric Chart of the Ocean (GEBCO) Compilation Group, 2023, GEBCO Grid.

Gordon, A.L., 1989, Brazil-Malvinas Confluence–1984: Deep Sea Research, Part A., Oceanographic Research Papers, v. 36, pp. 359–384.

Gruetzner, J., Uenzelmann-Neben, G., and Franke, D., 2016, Evolution of the northern Argentine margin during the Cenozoic controlled by bottom-current dynamics and gravitational processes: Geochemistry, Geophysics, Geosystems, v. 17, pp. 3131–3149.

Gruetzner, J., Uenzelmann-Neben, G., and Franke, D., 2012, Variations in sediment transport at the central Argentine continental margin during the Cenozoic: Geochemistry Geophysics Geosystems, v. 13, pp. 405-417.

Gruetzner, J., Uenzelmann-Neben, G., and Franke, D., 2011, Variations in bottom water activity at the southern Argentine margin: indications from a seismic analysis of a continental slope terrace: Geo-Marine Letters, v. 31, pp. 405–417.

Hernández-Molina, F.J., de Castro, S., de Weger, W., Duarte, D., Fonnesu, M., Glazkova, A., Kirby, A., Llave, E., Ng, Z.L., Mantialla Munoz, O., Rodrigues, S., Rodriguez-Tovar, F.J., Thieblemont, A., Viana, A., and Yin, S., 2022, Chapter 9 -Contourites and mixed depositional systems: A paradigm for deepwater sedimentary environments, *in* Rotzien, J.R., Yeilding, C.A., Sears, R.A., Hernández-Molina, F.J., and Catuneanu, O. eds., Deepwater Sedimentary Systems: Elsevier, pp. 301–360.

Hernández-Molina, F.J., Wahlin, A., Bruno, M., Ercilla, G., Llave, E., Serra, N., Roson, G., Puig, P., Rebesco, M., Rooij, D., Roque, D., Gonzalez-Pola, C., Sanchez, F., Ballesteros, M., Preu. B., Schwenk, T., Hanebuth, T., Sanchez, R.F., Lafuente, J., and Sanchez-Gonzalez, J., 2015, Oceanographic processes and morphosedimentary products along the Iberian margins: A new multidisciplinary approach: Marine Geology, v. 378, pp. 127–156.

Hernandéz-Molina, F.J., Paterlini, M., Somoza, L., Violante, R.A., Arecco, M.A., de Isasi, M., Rebesco, M., Uenzelmann-Neben, G., Neben, S., and Marshall, P., 2010, Giant mounded drifts in the Argentine Continental Margin: Origins, and global implications for the history of thermohaline circulation: Marine and Petroleum Geology, v. 27, pp. 1508–1530.

Hernández-Molina, F.J., Paterlini, M., Violante, R.A., Marshall, P., de Isasi, M., Somoza, L., and Rebesco, M., 2009, Contourite depositional system on the Argentine Slope: An exceptional record of the influence of Antarctic water masses: Geology, v. 37, pp. 507–510.

Hernandéz-Molina, F.J., Llave, E., and Stow, D.A.V., 2008, Chapter 19 Continental Slope Contourites: Elsevier, Developments in Sedimentology, v. 60, pp. 379–408.

Hinz, K., Neben, S., Schreckenberger, B., Roeser, H.A., Block, M., de Souza, K.G., and Meyer, H., 1999, The Argentine continental margin north of 48°S: sedimentary successions, volcanic activity during breakup: Marine and Petroleum Geology, v. 16 (1), pp. 1–25.

Kasten, S., Schwenk, T., Aromokeye, D A., Baques, M., Baumann, K.H., Bergenthal, M., Bösche, J , Bozzano, G., Brune, R., Bülten, J., Chiessi, C.M., Coffinet, S., Crivellari, S., Dehning, K., Dohrmann, I., Dröllner, M., Düßmann, R., Durica, J.T., Frederichs, T., Garcia Chapori, N., Gonzales, L.N., Hanebuth, T.J.J., Hilgenfeldt, C., Hüttich, D., Jones, C.K., Klann, M., Klar, S., Klein, T., Kockisch, B., Köster, M., Lantzsch, H., Linowski, E., Long, J. H., Melcher, A. C., Ogunleye, O.J., Pereyra, N., Rehage, R., Riedinger, N., Rosiak, U., Schmidt, W., Schnakenberg, A., Spiess, V., Steinmann, L., Thieblemont, A., Volz, J., Warnke, F., Warratz, G., Wenau, S., and Zonneveld, K.A., 2019, Dynamics of sedimentation processes and their impact on biochemical reactions on the continental slope off Argentina and Uruguay (MARUM), Cruise No. 260/Leg 1 & Leg 2: January 12-January 30, 2018, Buenos Aires (Argentina) -Montevideo (Uruguay), Leg 2: February 2 -February 14, 2018, Montevideo (Uruguay) -Buenos Aires (Argentina). DosProsBio, Sonne-Berichte.

Katz, M.E., Cramer, B.S., Toggweiler, J.R., Esmay, G., Liu, C., Miller, K.G., Rosenthal, Y., Wade, B.S., and Wright, J.D., 2011, Impact of Antarctic Circumpolar Current Development on Late Paleogene Ocean Structure: Science, v. 332, pp. 1076–1079.

Kennett, J.P., Keller, G., and Srinivasan, M.S., 1985, Miocene planktonic foraminiferal biogeography and paleoceanographic development of the Indo-Pacific region, The Miocene Ocean: Paleoceanography and Biogeography, James P. Kennett.

Kirby, A., Hernandéz-Molina, F.J., Rodriguez, P., and Conti, B., 2021, Sedimentary stacking pattern of plastered drifts: An example from the Cenozoic on the Uruguayan continental slope: Marine Geology, v. 440, pp. 106-567.

Krastel, S., and Wefer, G., 2011, Sediment transport off Uruguay and Argentina: From the shelf to the deep sea -Cruise No. M78/3 -May 19 -July 06, 2009 -Montevideo (Uruguay) -Montevideo (Uruguay): METEOR-Berichte, pp. 1–58.

Liu, S., Hernández-Molina, F.J., Ercilla, G., and Van Rooij, D., 2020, Sedimentary evolution of the Le Danois contourite drift systems (southern Bay of Biscay, NE Atlantic): A reconstruction of the Atlantic Mediterranean Water circulation since the Pliocene: Marine Geology, v. 427, pp. 106-217.

Llave, E., Schönfeld, J., Hernández-Molina, F.J., Mulder, T., Somoza, L., Del Río, V.D., and Sánchez-Almazo, I., 2006. High-resolution stratigraphy of the Mediterranean outflow contourite system in the Gulf of Cadiz during the late Pleistocene: the impact of Heinrich events: Marine Geology, v. 227(3-4), pp. 241-262.

Loegering, M.J., Anka, Z., Autin, J., di Primio, R., Marchal, D., Rodriguez, J.F., Franke, D., and Vallejo, E., 2013, Tectonic evolution of the Colorado Basin, offshore Argentina, inferred from seismo-stratigraphy and depositional rates analysis: Tectonophysics, v. 604, pp. 245–263.

Miramontes, E., Thiéblemont, A., Babonneau, N., Penven, P., Raisson, F., Droz, L., Jorry, S., Fierens, R., Counts, J., Wilckens, H., Cattaneo, A., and Gwenael, J., 2021, Contourite and mixed turbidite-contourite systems in the Mozambique Channel (SW Indian Ocean): Link between geometry, sediment characteristics and modelled bottom-currents: Marine Geology, v. 437, pp. 106-502.

Miramontes, E., Garreau, P., Caillaud, M., Jouet, G., Pellen, R., Hernández-Molina, F. J., Clare, M.A., and Cattaneo, A., 2019, Contourite distribution and bottom-currents in the NW Mediterranean Sea: Coupling seafloor geomorphology and hydrodynamic modelling. Geomorphology, v. 333, pp. 43–60.

Miramontes, E., Cattaneo, A., Jouet, G., Thereau, E., Thomas, Y., Rovere, M., Cauquil, E., and Trincardi, F., 2016, The Pianosa Contourite Depositional System (Northern Tyrrhenian Sea): Drift morphology and Plio-Quaternary stratigraphic evolution. Marine Geology, v. 378, pp. 20–42.

Mitchum, R.M.J., Vail, P.R., and Sangree, J.B., 1977, Stratigraphic Interpretation of Seismic Reflection Patterns in Depositional Sequences, in: Payton, C.E., Ed., Seismic Stratigraphy: Applications to Hydrocarbon Exploration, American Association of Petroleum Geologist (AAPG) Memoir 26, pp. 117-133.

Peterson, R.G., and Stramma, L., 1991, Upper-level circulation in the South Atlantic Ocean: Progress in Oceanography, v. 26, pp. 1–73.

Piola, A.R., and Matano, R.P., 2019, Ocean Currents: Atlantic Western Boundary—Brazil Current/Falkland (Malvinas) Current, *in* Cochran, J.K., Bokuniewicz, Henry.J., and Yager, Patricia.L. eds., Encyclopedia of Ocean Sciences (Third Edition), Oxford, Academic Press, pp. 414–420.

Piola, A.R., and Gordon, A.L., 1989, Intermediate waters in the southwest South Atlantic: Deep Sea Research Part A. Oceanographic Research Papers, v. 36 (1), pp. 1–16.

Preu, B., Hernández-Molina, F.J., Violante, R.A., Piola, A.R., Paterlini, C.M., Schwenk, T., Voigt, I., Krastel, S., and Spiess, V., 2013, Morphosedimentary and hydrographic features of the northern Argentine margin: The interplay between erosive, depositional and gravitational processes and its conceptual implications: Deep Sea Research Part I: Oceanographic Research Papers, v. 75, pp. 157–174.

Preu, B., Schwenk, T., Hernández-Molina, F.J., Violante, R.A., Paterlini, C.M., Krastel, S., Tomasini, J., and Spiess, V., 2012, Sedimentary growth pattern on the northern Argentine slope: The impact of North Atlantic Deep Water on southern hemisphere slope architecture: Marine Geology, v. 329, pp. 113–125.

Rebesco, M., Hernandéz-Molina, F.J., Van Rooij, D., and Wåhlin, A., 2014, Contourites and associated sediments controlled by deep-water circulation processes: state-of-the-art and future considerations: Marine Geology, v. 352. pp. 111-154.

Rebesco, M., Camerlenghi, A., and van Loon, A.J., 2008, Chapter 1 Contourite Research: A Field in Full Development: Elsevier, Developments in sedimentology, v. 60, pp. 1–10.

Rebesco, M., 2005, Contourites R.C. Selley, L.R.M. Cocks, I.R. Pilmer (Eds.), Encyclopedia of Geology, Elsevier, Oxford, pp. 513-527.

Rebesco, M., and Stow, D.A.V., 2001, Seismic expression of contourites and related deposits: a preface: Marine Geophysical Researches, v. 22, pp. 303–308.

Rodrigues, S., Hernandéz-Molina, F.J., Fonnesu, M., Miramontes, E., Rebesco, M., and Campbell, D.C., 2022, A new classification system for mixed (turbidite-contourite) depositional systems: Examples, conceptual models and diagnostic criteria for modern and ancient records: Earth-Science Reviews, v. 230 (1), 104030.

Rodrigues, S., Hernandéz-Molina, F.J., and Kirby, A., 2020, A Late Cretaceous mixed (turbidite-contourite) system along the Argentine Margin: Paleoceanographic and conceptual implications: Marine and Petroleum Geology, v. 123, pp. 104-768.

Smillie, Z., Stow, D.A.V., and Esentia, I.P., 2018, Deep-sea contourites drifts, erosional features and bedforms: Science Direct, Encyclopedia of Ocean Sciences, Third Edition Reference Module in Earth Systems and Environmental Sciences, v.4, pp. 97-110.

Spiess, V., Albrecht, N., Bickert, T., Breitzke, M., Brüning, M., Dreyzehner, A., Groß, U., Krüger, D., von Lom-Keil, H., and Möller, H., 2002, ODP Südatlantik 2001 Part 2. Meteor Berichte 2, 1.

Steinmann, L., Baques, M., Wenau, S., Schwenk, T., Spiess, V., Piola, A.R., Bozzano, G., Violante, R.A., and Kasten, S., 2020, Discovery of a giant cold-water coral mound province along the northern Argentine margin and its link to the regional Contourite Depositional System and oceanographic setting: Marine Geology, v. 427, pp. 106-223.

Stow, D.A.V., and Smillie, Z., 2020, Distinguishing between deep-water sediment facies: Turbidites, contourites and hemipelagites: Geoscience, v. 10, 68 p.

Stow, D.A.V., Faugères, J.-C., Howe, J.A., Pudsey, C.J., and Viana, A.R., 2002, Bottom-currents, contourites and deep-sea sediment drifts: current state-of-the-art. In Memoirs, vol. 22, pp. 7-20.

Stramma, L., and England, M., 1999, On the water masses and mean circulation of the South Atlantic Ocean: Journal of Geophysical Research: Oceans, v. 104, pp. 20.863–20.883.

Thiéblemont, A., Hernández-Molina, F.J., Miramontes, E., Raisson, F., and Penven, P., 2019, Contourite depositional systems along the Mozambique channel: The interplay between bottom-currents and sedimentary processes: Deep Sea Research Part I: Oceanographic Research Papers, v. 147, pp. 79–99.

Uenzelmann-Neben, G., Weber, T., Grützner, J., and Thomas, M., 2017, Transition from the Cretaceous ocean to Cenozoic circulation in the western South Atlantic — A twofold reconstruction: Tectonophysics, v. 716, pp. 225–240.

Urien, C.M., and Zambrano, J.J., 1973, The Geology of the Basins of the Argentine Continental Margin and Malvinas Plateau. In: Nairn, A.E.M., Stehli, F.G. (eds) The South Atlantic. Springer, pp. 135–169.

Violante, R.A., Paterlini, C.M., Costa, I.P., Hernández-Molina, F.J., Segovia, L.M., Cavallotto, J.L., Marcolini, S., Bozzano, G., Laprida, C., Chapori, N.G. and Bickert, T., 2010, Sismoestratigrafia y evolución geomorfológica del talud continental adyacente al litoral del este bonaerense, Argentina: Latin American Journal of Sedimentology and Basin Analysis, v. 17 (1), pp. 33–62.

Voigt, I., Henrich, R., Preu, B., Piola, A.R., Hanebuth, T.J.J., Schwenk, T., and Chiessi, C.M., 2013, A submarine canyon as a climate archive — Interaction of the Antarctic Intermediate Water with the Mar del Plata Canyon (Southwest Atlantic): Marine Geology, v. 341, pp. 46–57.

Warnke, F., Schwenk, T., Miramontes, E., Spiess, V., Wenau, S., Bozzano, G., Baqúes, M., and Kasten, S., 2023, Evolution of complex giant seafloor depressions at the northern Argentine continental margin (SW Atlantic Ocean) under the influence of a dynamic bottom-current regime: Frontiers in Earth Science: Marine Geoscience, v. 11, pp. 1–54.

Warratz, G., Schwenk, T., Voigt, I., Bozzano, G., Henrich, R., Violante, R.A., and Lantzsch, H., 2019, Interaction of a deep-sea current with a blind submarine canyon (Mar del Plata Canyon, Argentina): Marine Geology, v. 417, 106002.

Wilckens, H.., Schwenk, T., Lüdmann, T., Betzler, C., Zhang, W., Chen, J., Hernández-Molina, F.J., Lefebvre, A., Cattaneo, A., Spiess, V., and Miramontes, E., 2023a, Factors controlling the morphology and internal sediment architecture of moats and their associated contourite drifts: Sedimentology, v. 70, pp. 1–31.

Wilckens, H., Eggenhuisen, J.T., Adema, P.H., Hernández-Molina, F.J., Jacinto, R.S., and Miramontes, E., 2023b, Secondary flow in contour currents controls the formation of moat-drift contourite systems: Communications Earth & Environment, v. 4, pp. 1–10.

Wilckens, H., Miramontes, E., Schwenk, T., Artana, C., Zhang, W., Piola, A., Baques, M., Provost, C., Hernández-Molina, F.J., Felgendreher, M., Spiess, V., and Kasten, S., 2021, The erosive power of the Malvinas Current: Influence of bottom-currents on morpho-sedimentary features along the northern Argentine margin (SW Atlantic Ocean): Marine Geology v. 439, pp. 106-539.

Zhao, Y., Liu, Z., Zhang, Y., Zhang, X., Ma, P., Yu, X., Liang, C., Lin., B., and Zhang, J., 2024, Formation mechanism of drift-moat contourite systems revealed by in-situ observations in the South China Sea: Earth and Planetary Science Letters, v. 628, 118585.

FIGURE CAPTIONS

Figure 1: A) Overview map of the Argentine Margin showing the primary circulation pattern in the area (from Hernández-Molina et al., 2009; Preu et al., 2012; Wilckens et al., 2021). Black dots indicate the approximate position of two industrial boreholes (Sb-III SAMAR-D x-1 and Dorado x-1) considered in Violante et al. (2010). Background bathymetry is the IBCSO v2 (Dorschel et al., 2022). AAIW: Antarctic Intermediate Water, CDW: Circumpolar Deep Water, NADW: North Atlantic Deep Water, AABW: Antarctic Bottom Water, BMC: Brazil-Malvinas Confluence Zone. B) Regional bathymetric map from the GEBCO 2023 Grid (GEBCO Compilation Group, 2023) is overlain by processed multibeam bathymetry acquired during cruise SO260, available at DOI:

10.1594/PANGAEA.88569. The relevant seismic profiles for this study (GeoB18-036, -032, -038 and -073) are indicated with black lines. Outline of Ewing Terrace Moat-1 and -2 (ET-1 and -2) from Steinmann et al. (2020) and Wilckens et al. (2021) and Seafloor Depression-S and -N (SD-S and SD-N) from Warnke et al. (2023) are shown with dashed white lines. C) Flow direction and extension of the modern-day bottom water masses at the Ewing Terrace (colored). The oceanographic setting is pointed out with colored arrows, showing the intermediate and deep-water circulation along the southwest Atlantic margin (from Warratz et al., 2019 and Wilckens et al., 2021;). Red: NADW, green: CDW (LCDW and UCDW), blue: AAIW and white: MC2 and 3 (adapted from Preu et al., 2013; Steinmann et al., 2020; Wilckens et al., 2021). LCDW: Lower Circumpolar Deep Water, UCDW: Upper Circumpolar Deep Water, MC: Malvinas Current.

Figure 2: Interpreted seismic profile GeoB18-036 crossing the paleo-moat in the northern part of the Southern Ewing Terrace. AR3-AR8: colored key reflections separating seismostratigraphic units SU1-SU7 correlated from Violante et al. (2010), Preu et al. (2012) and Gruetzner et al. (2016). The current direction is into the page, and a northward flow is evident. Red zones are transparent areas. HAR: High-amplitude reflection. See Figure S1 for the uninterpreted version of the seismic profile.

Figure 3: Overview of the regional seismostratigraphy and depositional units at the study area, correlated to three previous stratigraphic schemes, tectonic events, paleoclimate and -oceanography of the Southern Ewing Terrace (from Violante et al., 2010; Preu et al., 2012; Gruetzner et al., 2016 and references therein). SD: Depositional Sequence, SU: Seismic Unit, CAS: Central American Seaway, DP: Drake Passage, NADW: North Atlantic Deep Water, CDW: Circumpolar Deep Water, BMC: Brazil-Malvinas-Confluence Zone, ACC. Antarctic Circumpolar Current, UPW: Upper Pacific Water, ACM: Argentine Continental Margin, MMCO: Mid-Miocene Climatic Optimum.

Figure 4: A) 2-D view of the paleo bathymetry from seismic reflector AR4 (Eocene/Oligocene boundary), which marks the lower boundary of the investigated paleo-moat. B) Isopach map shows the sediment thickness between AR4 and AR5 (Eocene/Oligocene boundary to Early/Middle Miocene boundary) of Seismic Unit 3 (SU3) in the study area, derived from all available seismic profiles from

SO260 covering the Southern Ewing Terrace, including the seismic profiles relevant for this study. Time-to-depth conversion was calculated based on a constant sound velocity of 1500 m/s.

Figure 5: A) Interpreted seismic profile GeoB18-036 showing the paleo-moat's internal architecture within the Southern Ewing Terrace subseafloor. AR4-AR8 separate the key seismic units following the seismostratigraphic framework of Violante et al. (2010), Preu et al. (2012) and Gruetzner et al. (2016). Moat-drift (M-D) systems are outlined with black lines. B) Line drawing of two measured moat-drift systems (M-D2 and -3), that show the measured moat-drift parameters inferred from A) respectively. See Figure S2 for the uninterpreted full seismic profiles.

Figure 6: A) and C) Interpreted seismic profiles GeoB18-038 and -032 showing the internal architecture of SU3 at the central SET with a distance of 10 km to each other. Both show three moat-drift systems (M-D1-3) outlined with black lines. AR3-AR7 separate the seismic units (A) based on stratigraphic framework of Violante et al. (2010), Preu et al. (2012) and Gruetzner et al. (2016). B) and D) Line drawing of the M-D systems identified in the seismic profiles. See Figure S2 and S3 for the uninterpreted full seismic profiles.

Figure 7: A) W-E oriented seismic profile GeoB18-073 crossing the southern area of the SET. The paleo-moat is located in SU3. AR3- AR6 mark the key horizons, indicated with colored lines and separated by seismic units SU1-SU5. B) Line drawing of M-D systems and their measured parameters. One M-D1 system can be measured from GeoB18-073. See Figure S3 for the uninterpreted full seismic profiles.

Figure 8: The figure presents a series of scatter plots (A-E) and a data table (F) that explore the relationships between various geomorphological parameters of the identified M-D systems (Fig. 5-7). A) Shows the relationship between relief (m) and width (m), revealing a positive correlation (R^2=0.92), indicating that as the width increases, the relief also increases. B) Illustrates the relationship between slope angle (°) and width (m), with a negative correlation (R^2=-0.38) suggesting that wider systems may have a lower slope angle. C) Shows slope angle (°) over relief (m), showing a weak positive correlation (R^2=0.25), suggesting that a greater relief tends to have steeper slope angles. D) Depicts the relationship between slope angle (°) and the ratio of relief to width (R-W ratio; m),

showing a moderate correlation (R^2=0.50). E) Shows the relationship between slope angle (°) and drift angle (°) with no correlation (R^2=0.01). Finally, Table F) lists the M-D systems analyzed, providing values for relief (m), width (m), slope angle (°), drift angle (°) and R-W ratio (m), which are the basis for the presented plots (A-E).

Figure 9: Shown is a conceptual model of the build-up of the buried moat in four consecutive sequences (Stages 1-4) at the Ewing Terrace during the Oligocene. The development of the Moat-Drift (M-D) systems was caused by the introduction of northward flowing currents at the Argentine Margin as displayed in Stage 1. During Stage 2 the southern sector developed one (M-D1) and the central sector three M-D systems (M-D1-3), which indicates a uniform deposition for that part of the area. Whereas the northernmost sector depicts a highly complex deposition with a high density of M-D systems (M-D1-8). The potential evolution scenario for the north is displayed in detail in the three zooms, deciphering the build-up of M-D 1-8. Due to differences in slope angles (see legend), the drift flanks are pronounced to varying degrees. The steeper the slope, the steeper the drift flanks/ drift angle, which is especially the case for the northern evolution as it differentiates compared to the southern and central M-D system build-up. The successive upslope migration is related to fluxes in the Brazil-Malvinas confluence zone and differences in current strength, thus the M-D system build-up differs over the Ewing Terrace, this can be observed in Stage 3. The final stage (Stage 4) shows that an offset of moat-drift development is reached after the slope angle reaches a minimum and the bottom current has the ability to broaden over the entire terrace. Please refer to the text for a detailed description of the evolution (*Moat-drift architecture and associated current dynamics).*

Figure 1

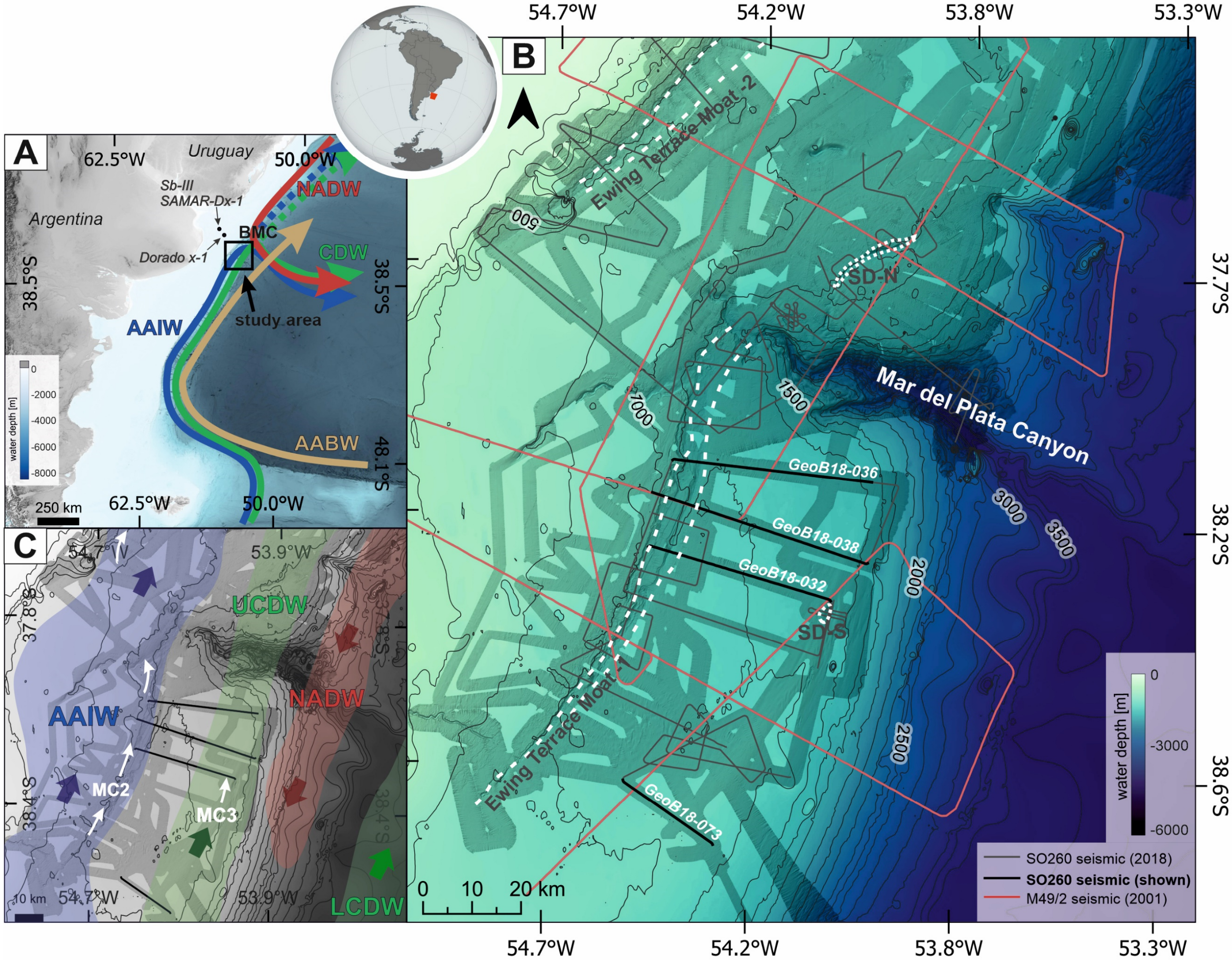

A
62.5°W
Uruguay
50.0°W
Sb-III
SAMAR-Dx-1
NADW
Argentina
BMC
Dorado x-1
CDW
38.5°S
38.5°S
study area
AAIW
water depth [m]
0
-2000
-4000
-6000
-8000
AABW
48.1°S
250 km
62.5°W
50.0°W
B
54.7°W
54.2°W
53.8°W
53.3°W
Ewing Terrace Moat -2
500
SD-N
37.7°S
1000
1500
Mar del Plata Canyon
GeoB18-036
GeoB18-038
GeoB18-032
3000
3500
38.2°S
2000
SD-S
Ewing Terrace Moat
2500
GeoB18-073
water depth [m]
0
-3000
-6000
38.6°S
0 10 20 km
SO260 seismic (2018)
SO260 seismic (shown)
M49/2 seismic (2001)
C
54.7°W
53.9°W
37.8°S
UCDW
NADW
AAIW
MC2
MC3
38.4°S
10 km
54.7°W
53.9°W
LCDW

Figure 2

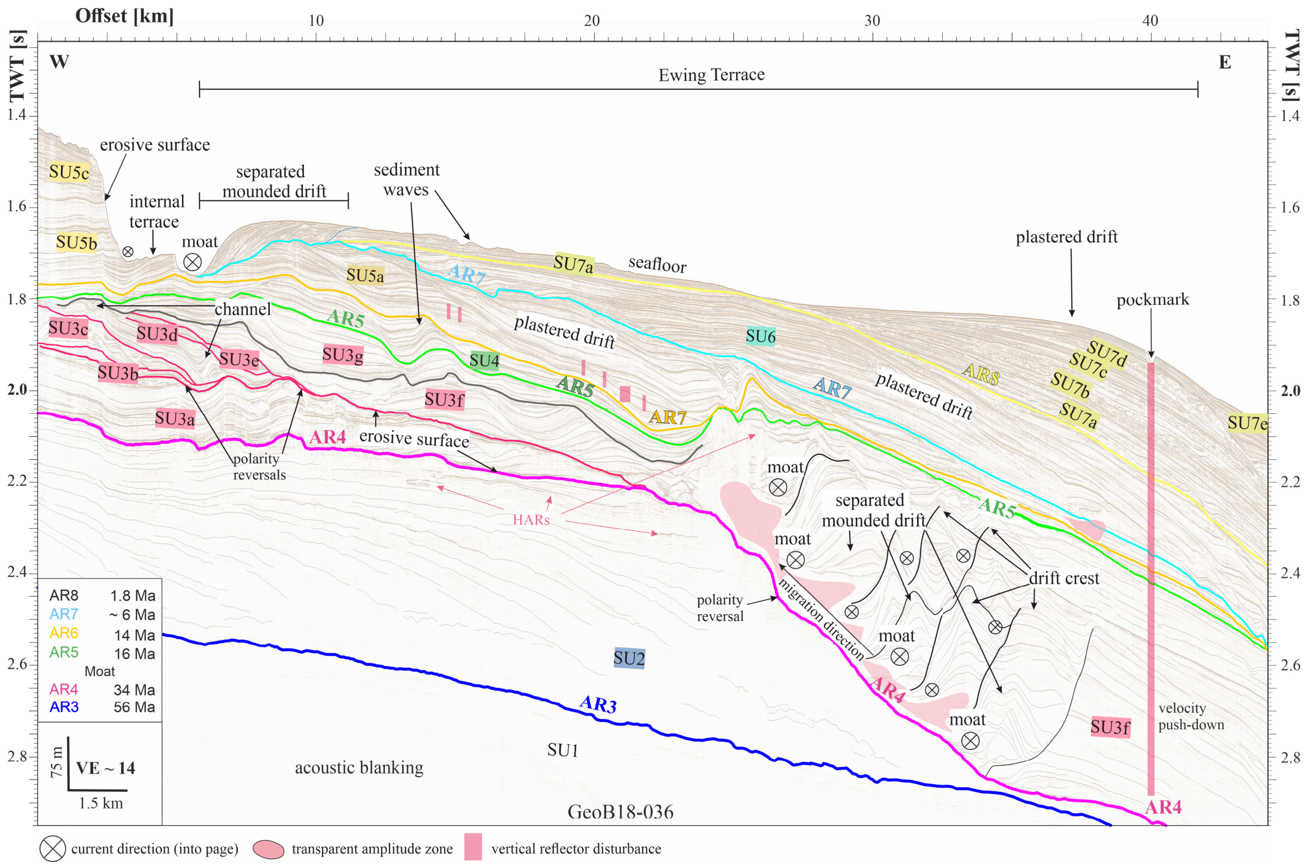

Offset [km]
10
20
30
40
TWT [s]
W
E
Ewing Terrace
erosive surface
SU5c
separated mounded drift
sediment waves
internal terrace
moat
SU5b
SU5a
AR7
SU7a
seafloor
plastered drift
pockmark
channel
SU3c
SU3d
AR5
SU3e
SU3g
plastered drift
SU6
SU7d
SU7c
SU7b
SU7a
AR8
SU3b
SU4
AR5
SU3f
AR7
AR7
plastered drift
SU7e
SU3a
AR4
erosive surface
polarity reversals
moat
HARs
separated mounded drift
AR5
moat
drift crest
polarity reversal
migration direction
moat
AR8 1.8 Ma
AR7 ~ 6 Ma
AR6 14 Ma
AR5 16 Ma
Moat
AR4 34 Ma
AR3 56 Ma
SU2
AR3
AR4
velocity push-down
moat
SU3f
75 m
VE ~ 14
1.5 km
SU1
acoustic blanking
GeoB18-036
AR4
current direction (into page)
transparent amplitude zone
vertical reflector disturbance

Figure 3

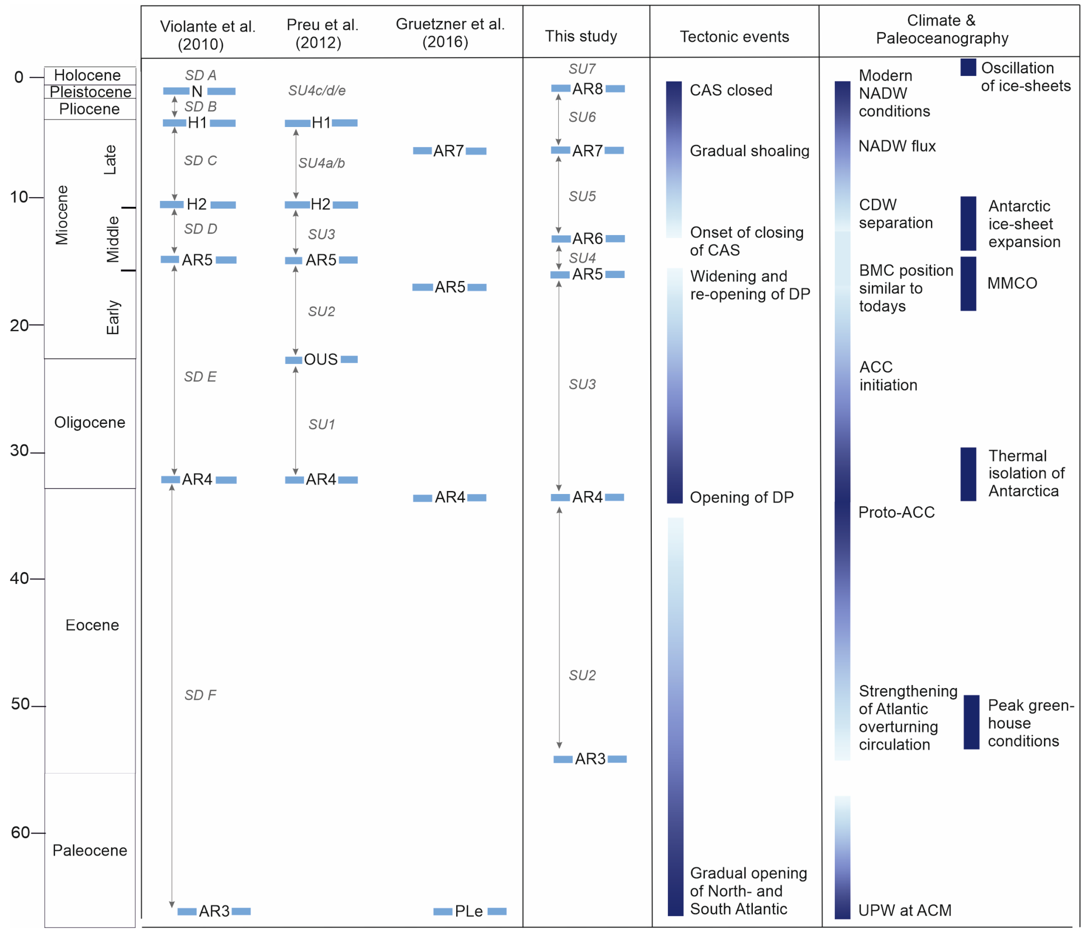

Violante et al. (2010)
Preu et al. (2012)
Gruetzner et al. (2016)
This study
Tectonic events
Climate & Paleoceanography
0
10
20
30
40
50
60
Holocene
Pleistocene
Pliocene
Miocene
Late
Middle
Early
Oligocene
Eocene
Paleocene
SD A
N
SD B
H1
SD C
H2
SD D
AR5
SD E
AR4
SD F
AR3
SU4c/d/e
H1
SU4a/b
H2
SU3
AR5
SU2
OUS
SU1
AR4
AR7
AR5
AR4
PLe
SU7
AR8
SU6
AR7
SU5
AR6
SU4
AR5
SU3
AR4
SU2
AR3
CAS closed
Gradual shoaling
Onset of closing of CAS
Widening and re-opening of DP
Opening of DP
Gradual opening of North- and South Atlantic
Modern NADW conditions
NADW flux
CDW separation
BMC position similar to todays
ACC initiation
Proto-ACC
Strengthening of Atlantic overturning circulation
UPW at ACM
Oscillation of ice-sheets
Antarctic ice-sheet expansion
MMCO
Thermal isolation of Antarctica
Peak green-house conditions

Figure 4

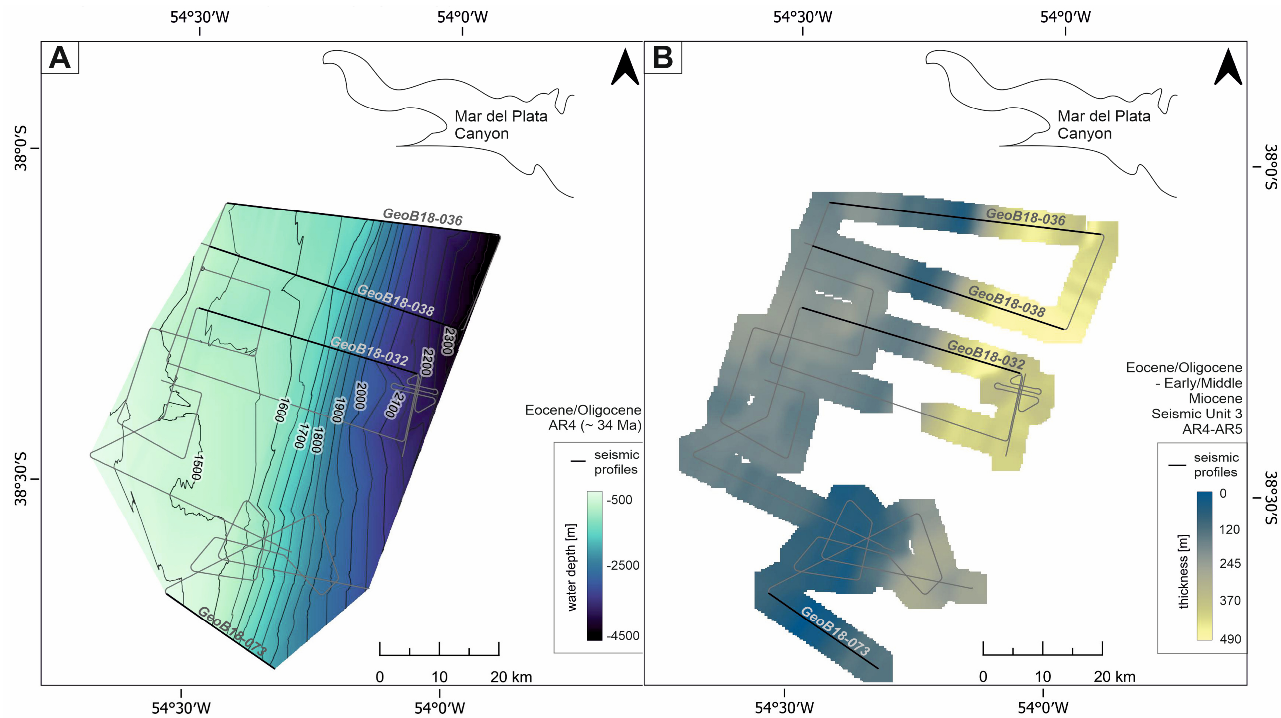

A
B
54°30′W
54°0′W
38°0′S
38°30′S
Mar del Plata
Canyon
GeoB18-036
GeoB18-038
GeoB18-032
GeoB18-073
1500
1600
1700
1800
1900
2000
2100
2200
2300
Eocene/Oligocene
AR4 (~ 34 Ma)
seismic
profiles
water depth [m]
-500
-2500
-4500
0
10
20 km
Eocene/Oligocene
- Early/Middle
Miocene
Seismic Unit 3
AR4-AR5
thickness [m]
0
120
245
370
490

Figure 5

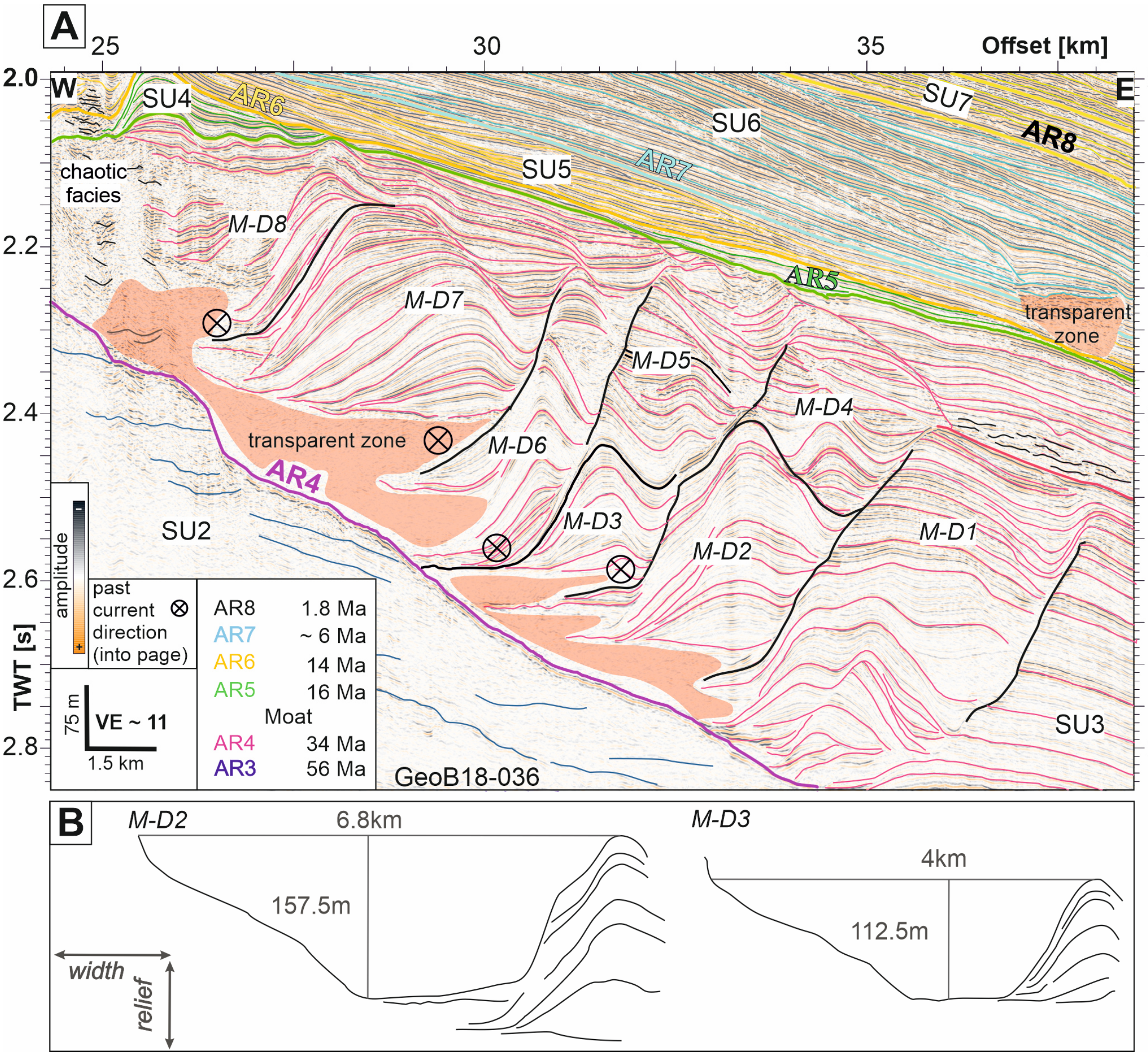

A
B
Offset [km]
25
30
35
2.0
2.2
2.4
2.6
2.8
TWT [s]
W
E
SU4
AR6
SU6
SU7
AR8
AR7
SU5
chaotic facies
M-D8
M-D7
AR5
transparent zone
M-D5
M-D4
transparent zone
M-D6
AR4
SU2
M-D3
M-D2
M-D1
SU3
amplitude
past current direction (into page)
AR8 1.8 Ma
AR7 ~ 6 Ma
AR6 14 Ma
AR5 16 Ma
Moat
AR4 34 Ma
AR3 56 Ma
75 m
VE ~ 11
1.5 km
GeoB18-036
M-D2
6.8km
157.5m
M-D3
4km
112.5m
width
relief

Figure 6

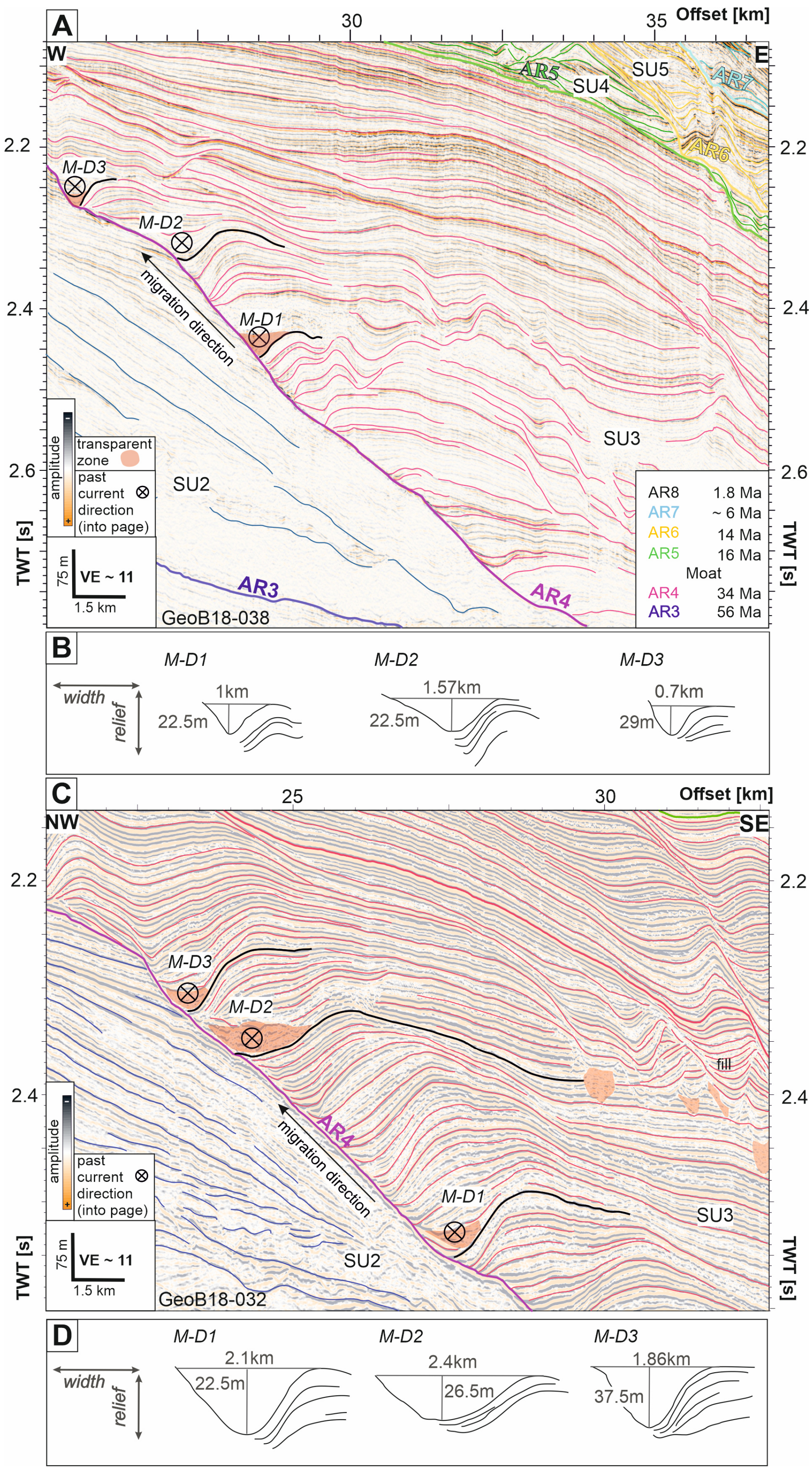

A
Offset [km]
30
35
W
E
AR5
SU4
SU5
AR7
AR6
2.2
M-D3
M-D2
migration direction
M-D1
2.4
amplitude
transparent zone
past current direction (into page)
SU2
SU3
2.6
TWT [s]
75 m
VE ~ 11
1.5 km
AR3
AR4
GeoB18-038
AR8 1.8 Ma
AR7 ~ 6 Ma
AR6 14 Ma
AR5 16 Ma
Moat
AR4 34 Ma
AR3 56 Ma
B
M-D1
M-D2
M-D3
width
relief
1km
22.5m
1.57km
22.5m
0.7km
29m
C
Offset [km]
25
30
NW
SE
2.2
M-D3
M-D2
fill
2.4
amplitude
past current direction (into page)
AR4
migration direction
M-D1
SU3
SU2
TWT [s]
75 m
VE ~ 11
1.5 km
GeoB18-032
D
M-D1
M-D2
M-D3
width
relief
2.1km
22.5m
2.4km
26.5m
1.86km
37.5m

Figure 7

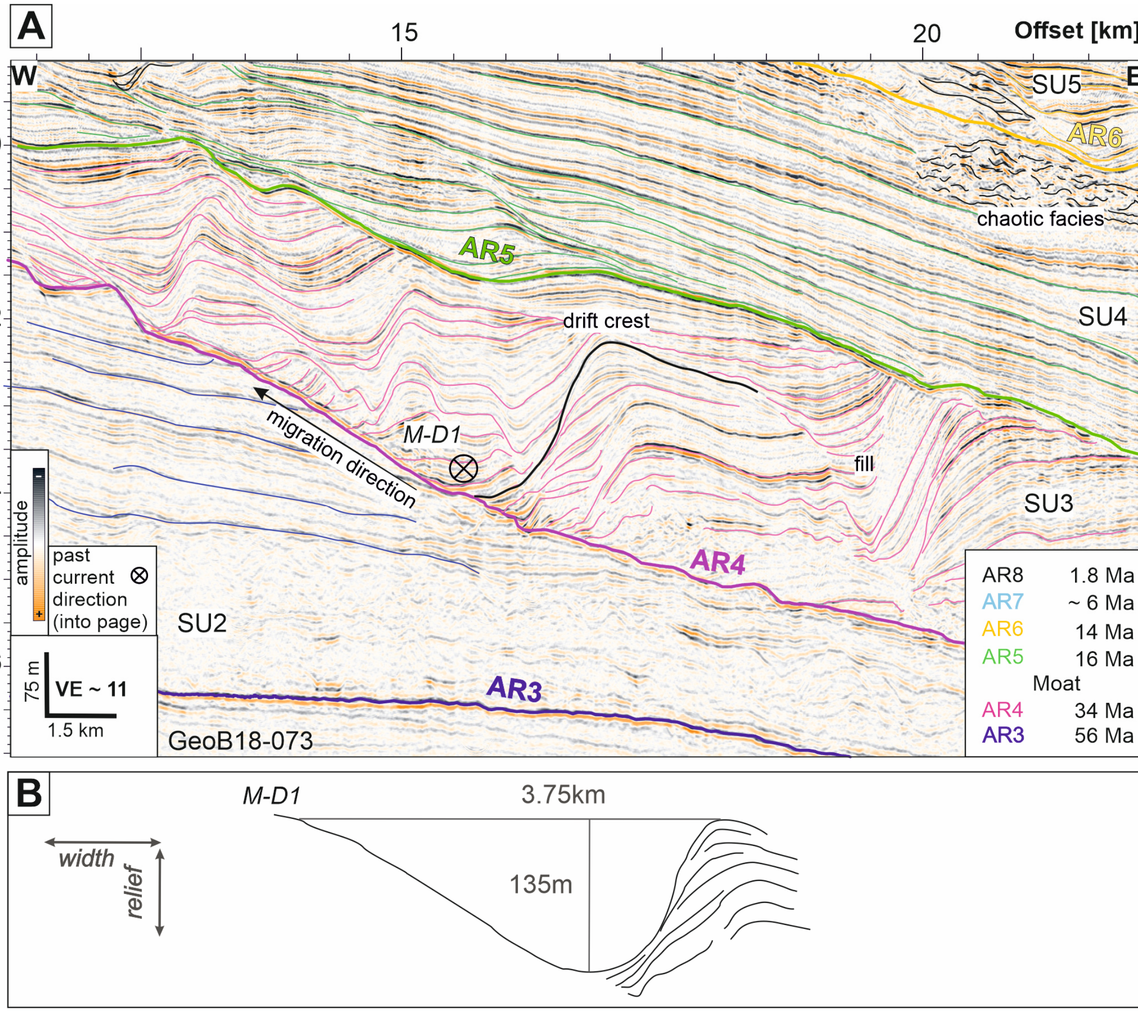

A
Offset [km]
15
20
W
E
SU5
AR6
chaotic facies
AR5
SU4
drift crest
migration direction
M-D1
fill
SU3
AR4
SU2
AR3
TWT [s]
2.0
2.2
2.4
2.6
amplitude
past current direction (into page)
75 m
VE ~ 11
1.5 km
GeoB18-073
AR8 1.8 Ma
AR7 ~ 6 Ma
AR6 14 Ma
AR5 16 Ma
Moat
AR4 34 Ma
AR3 56 Ma
B
M-D1
3.75km
135m
width
relief

Figure 8

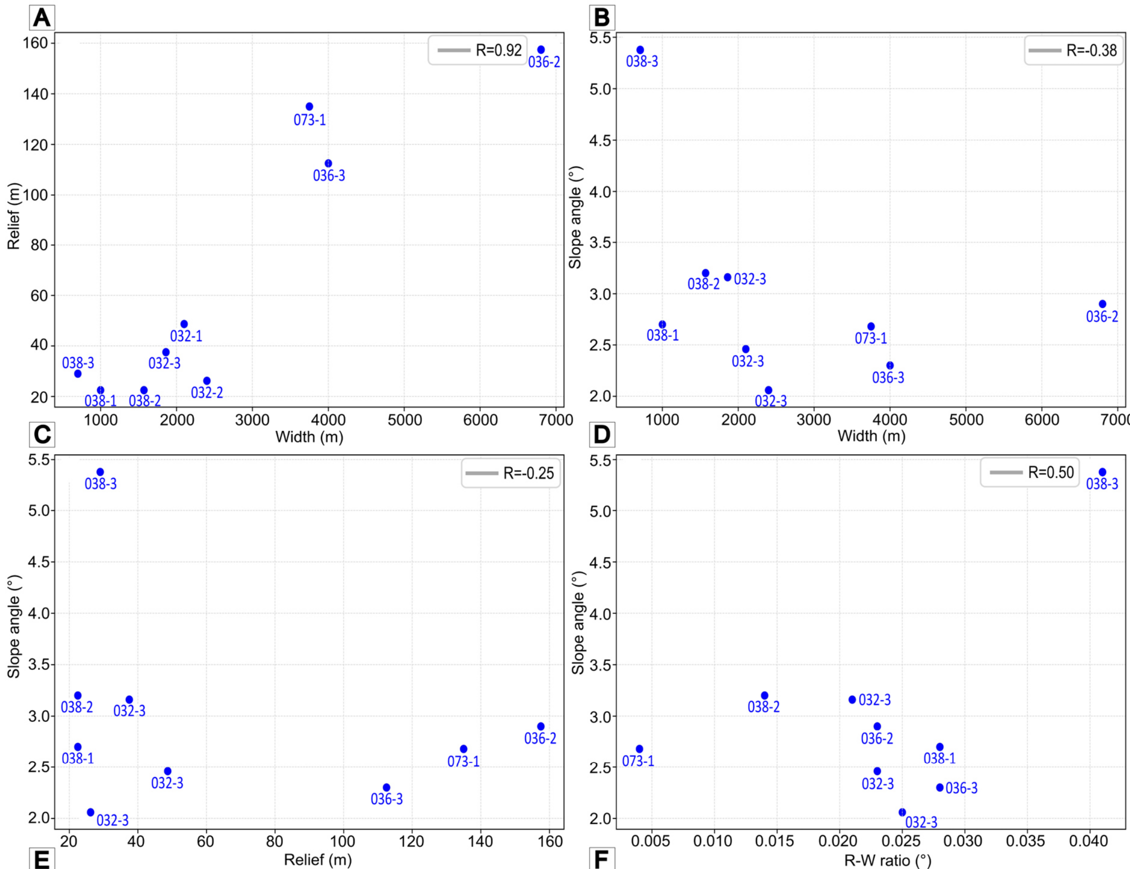

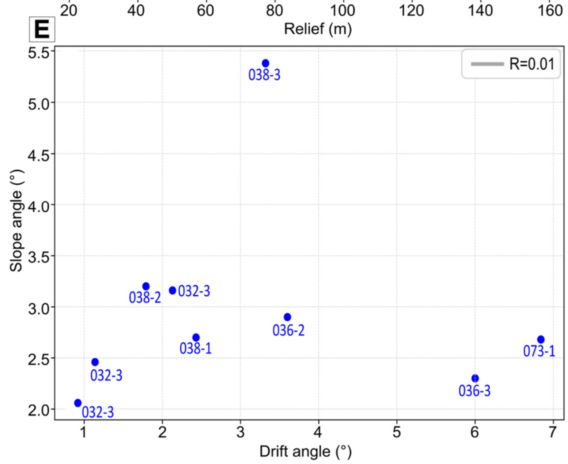

F

M-D systems	Relief (m)	Width (m)	Slope angle (°)	Drift angle (°)	R-W ratio (°)
073-1	135	3750	2.68	6.84	0.004
032-1	48.7	2100	2.46	1.14	0.023
032-2	26.2	2400	2.06	0.92	0.025
032-3	37.5	1860	3.16	2.13	0.021
038-1	22.5	1000	2.7	2.43	0.028
038-2	22.5	1570	3.2	1.79	0.014
038-3	29	700	5.38	3.32	0.041
036-2	157.5	6800	2.9	3.6	0.023
036-3	112.5	4000	2.3	6	0.028

Figure 9

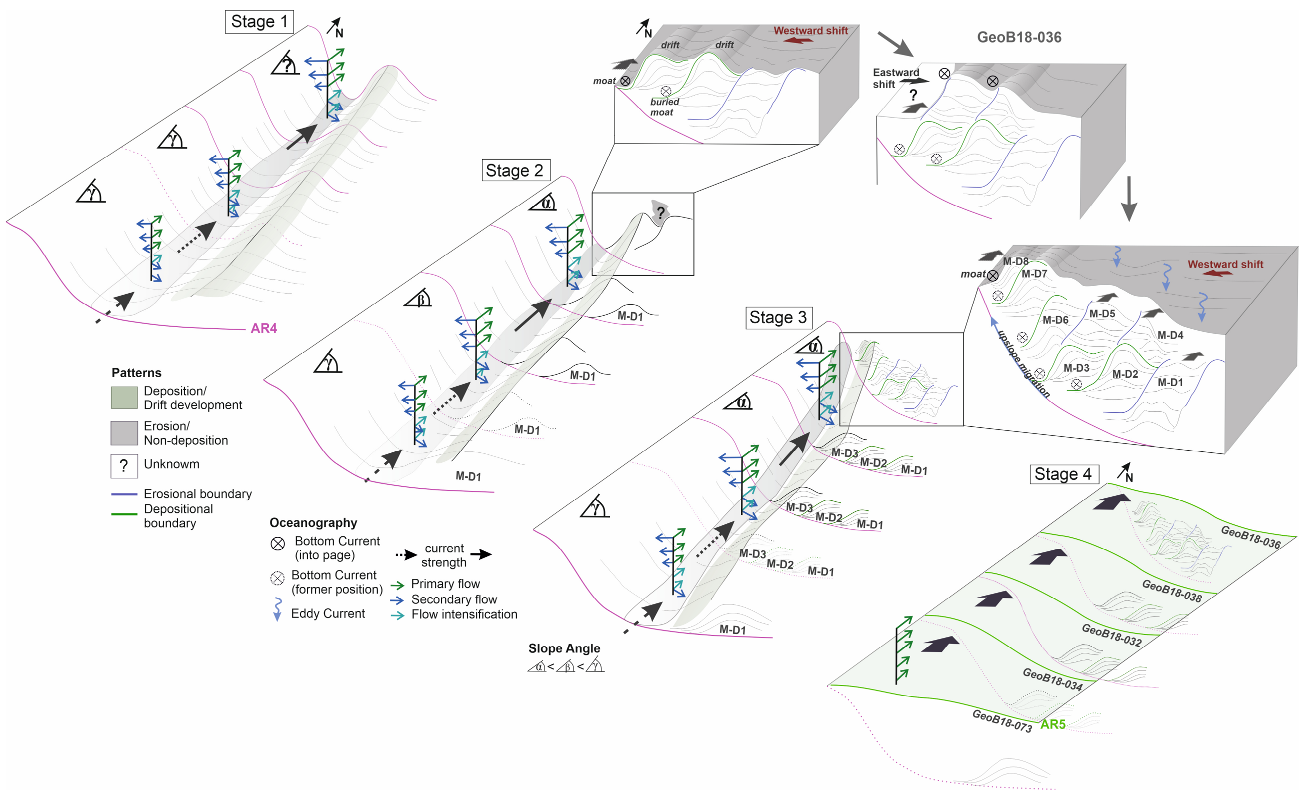
Stage 1
N
AR4
Stage 2
?
M-D1
M-D1
M-D1
M-D1
drift
drift
Westward shift
moat
buried moat
GeoB18-036
Eastward shift
?
Stage 3
M-D3
M-D2
M-D1
M-D3
M-D2
M-D1
M-D3
M-D2
M-D1
M-D1
moat
M-D8
M-D7
Westward shift
M-D6
M-D5
M-D4
M-D3
M-D2
M-D1
upslope migration
Stage 4
GeoB18-036
GeoB18-038
GeoB18-032
GeoB18-034
GeoB18-073
AR5
Patterns
Deposition/ Drift development
Erosion/ Non-deposition
Unknown
Erosional boundary
Depositional boundary
Oceanography
Bottom Current (into page)
Bottom Current (former position)
Eddy Current
current strength
Primary flow
Secondary flow
Flow intensification
Slope Angle

SUPPORTING INFORMATION

CONTENTS OF THIS FILE

INTRODUCTION

In the following, we present support information for the paper "Evolution of a buried moat-drift system within the Ewing Terrace uncovering highly dynamic bottom currents at the Argentine Margin during Early Oligocene.". Included are the processed and uninterpreted seismic profiles shown in Figures S1- S3.

FIGURE CAPTIONS

Figure S1. An uninterpreted version of seismic profile GeoB18-036 is shown in Figure 2.

Figure S2. An uninterpreted version of seismic sections A) GeoB18-036 and B) -038 is shown in Figure 5.

Figure S3. An uninterpreted version of seismic sections A) GeoB18-032 and B) -073 is shown in Figure 6.

Figure S1

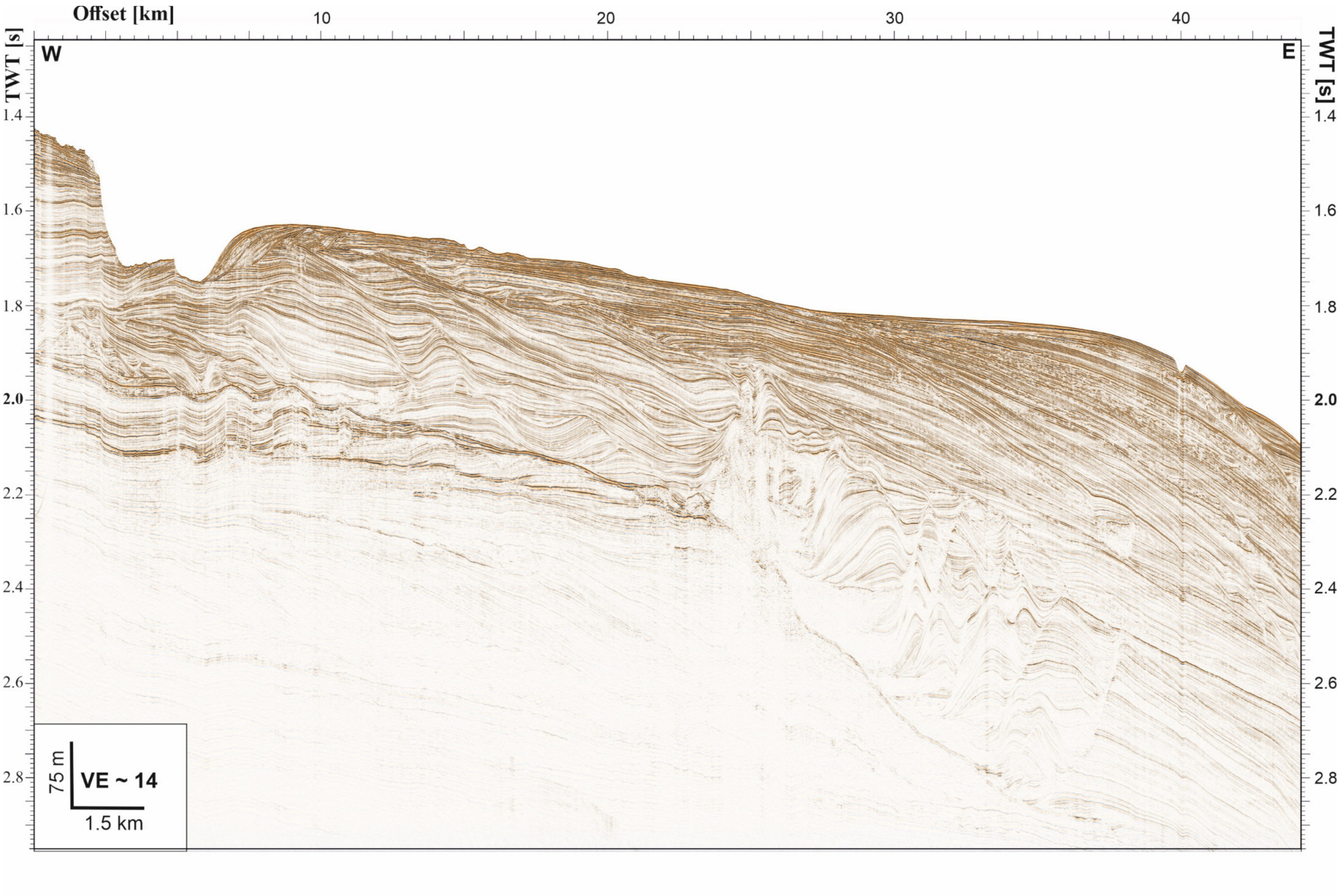
Offset [km]
10
20
30
40
W
E
TWT [s]
1.4
1.6
1.8
2.0
2.2
2.4
2.6
2.8
TWT [s]
75 m
VE ~ 14
1.5 km

Figure S2

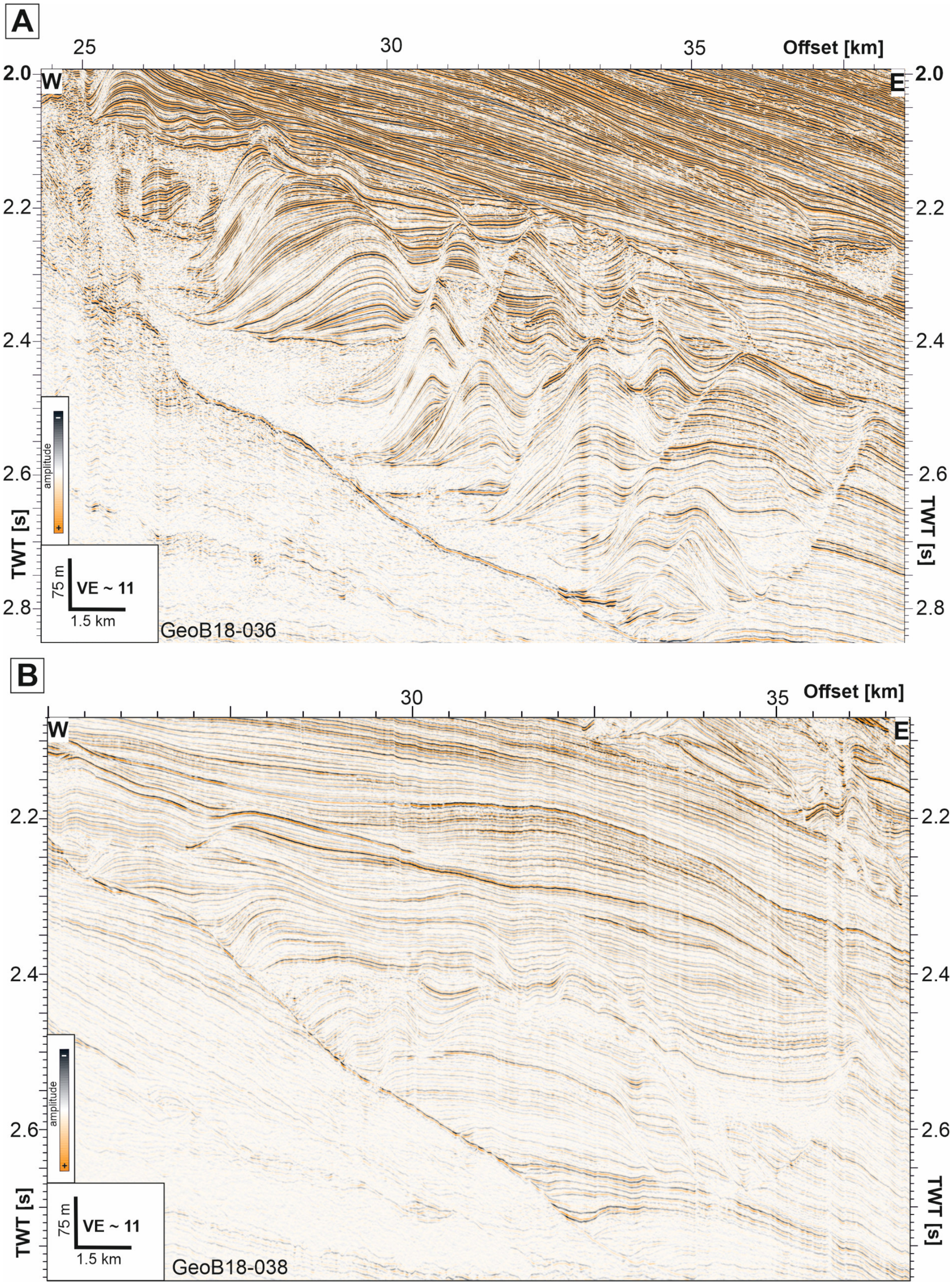
A
25
30
35
Offset [km]
W
E
2.0
2.2
2.4
2.6
2.8
TWT [s]
amplitude
75 m
VE ~ 11
1.5 km
GeoB18-036
B
30
35
Offset [km]
W
E
2.2
2.4
2.6
TWT [s]
amplitude
75 m
VE ~ 11
1.5 km
GeoB18-038

Figure S3

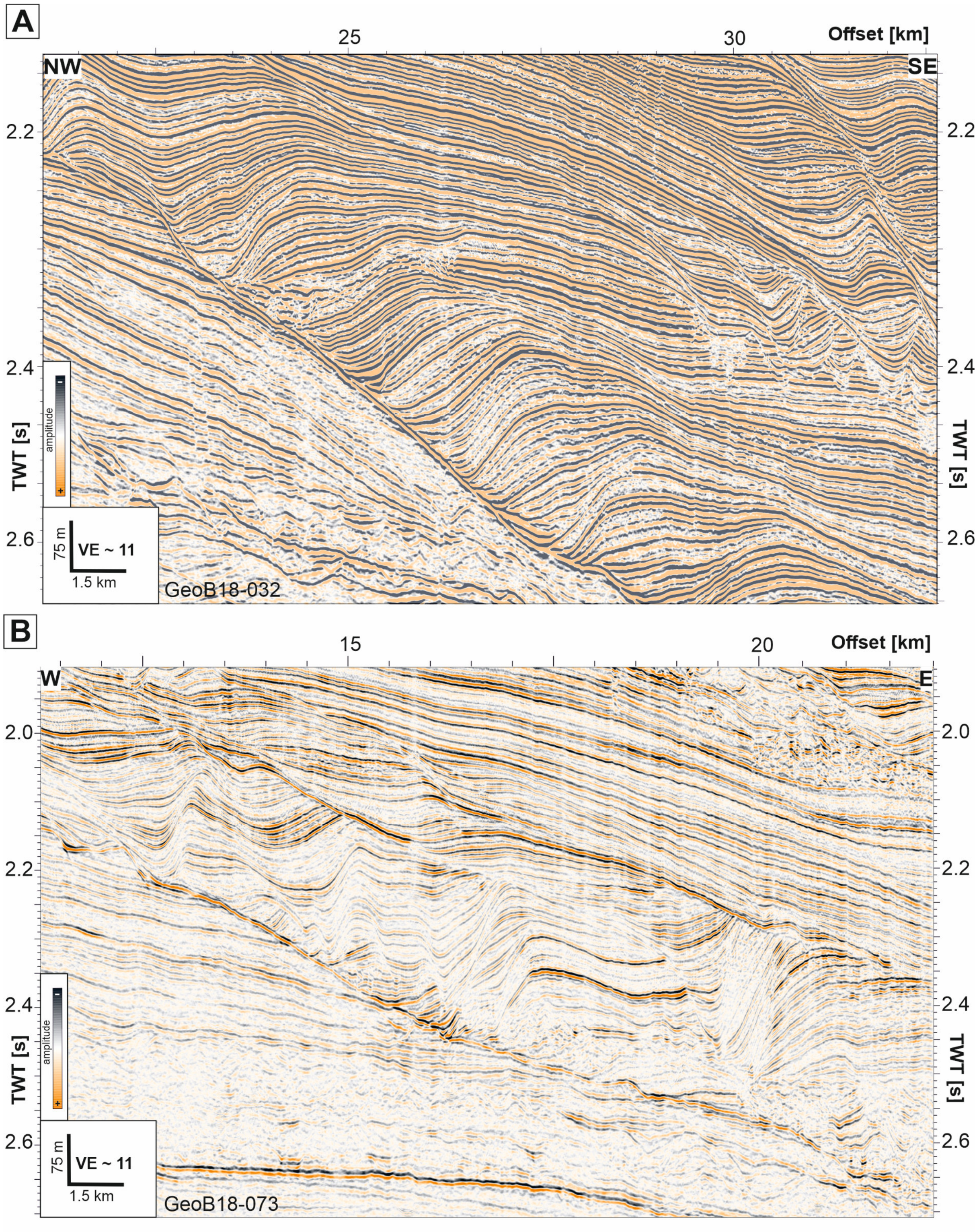
A
Offset [km]
25
30
NW
SE
2.2
2.4
2.6
TWT [s]
amplitude
75 m
VE ~ 11
1.5 km
GeoB18-032
B
Offset [km]
15
20
W
E
2.0
2.2
2.4
2.6
TWT [s]
amplitude
75 m
VE ~ 11
1.5 km
GeoB18-073